AMERICAN PSYCHOLOGICAL ASSOCIATION

Journal of Psychopathology and Clinical Science

ISSN: 2769-7541

2025, Vol. 134, No. 1, 41–56
https://doi.org/10.1037/abn0000940

Adolescent Social Anxiety Is Associated With Diminished Discrimination of Anticipated Threat and Safety in the Bed Nucleus of the Stria Terminalis

Juyoen Hur[1], Rachael M. Tillman[2], Hyung Cho Kim[3, 4], Paige Didier[3], Allegra S. Anderson[5], Samiha Islam[6], Melissa D. Stockbridge[7], Andres De Los Reyes[3], Kathryn A. DeYoung[3, 8], Jason F. Smith[3], and Alexander J. Shackman[3, 4, 9]

[1] Department of Psychology, Yonsei University
[2] Department of Neuropsychology, Children's National Hospital, Washington, District of Columbia, United States
[3] Department of Psychology, University of Maryland
[4] Neuroscience and Cognitive Science Program, University of Maryland
[5] Department of Psychological Sciences, Vanderbilt University
[6] Department of Psychology, University of Pennsylvania
[7] Department of Neurology, School of Medicine, Johns Hopkins University
[8] TheraQuest LLC, Bethesda, Maryland, United States
[9] Maryland Neuroimaging Center, University of Maryland

Social anxiety—which typically emerges in adolescence—lies on a continuum and, when extreme, can be devastating. Socially anxious individuals are prone to heightened fear, anxiety, and the avoidance of contexts associated with potential social scrutiny. Yet most neuroimaging research has focused on acute social threat. Much less attention has been devoted to understanding the neural systems recruited during the

This article was published Online First November 7, 2024.

Dylan Gee served as action editor.

Juyoen Hur https://orcid.org/0000-0002-6961-5199

Juyoen Hur and Rachael M. Tillman have contributed equally to this work.

This work was partially supported by the National Institutes of Health (AA030042, DA040717, MH107444, MH121409, MH131264); National Research Foundation of Korea (2021R1F1A106338513 and 2021S1A5A2A0307022913); and Yonsei Signature Research Cluster Program (2021-22-0005). All procedures were approved by the University of Maryland, College Park Institutional Review Board (Protocol 661215). The authors acknowledge assistance and critical feedback from J. Blanchard, L. Dougherty, N. Fox, L. Friedman, S. Grogans, C. Kaplan, B. Nacewicz, L. Pessoa, T. Riggins, B. Stephenson, Z. Tillman, members of the Affective and Translational Neuroscience Laboratory and Comprehensive Assessment and Intervention Program, and the staff of the Maryland Neuroimaging Center. The authors declare no conflicts of interest.

A preprint of this report is available at bioRxiv (https://www.biorxiv.org/content/10.1101/2023.10.30.564701v1).

Study materials, processed data, and statistical code are publicly available at https://osf.io/aj64g/.

Key neuroimaging maps are publicly available at https://neurovault.org/collections/15620.

Processed neuroimaging data have also been shared with the ENIGMA Consortium Anxiety Workgroup (https://enigma.ini.usc.edu/ongoing/enigma-anxiety). The data are available at https://osf.io/aj64g/ and https://neurovault.org/collections/15620.

Juyoen Hur served as lead for writing–review and editing and served in a supporting role for formal analysis. Rachael M. Tillman served as lead for project administration and writing–original draft. Hyung Cho Kim served in a supporting role for data curation, investigation, visualization, and writing–review and editing. Paige Didier served in a supporting role for investigation and writing–review and editing. Allegra S. Anderson served in a supporting role for data curation, investigation, project administration, and writing–review and editing. Samiha Islam served in a supporting role for data curation, investigation, project administration, and writing–review and editing. Melissa D. Stockbridge served in a supporting role for investigation, visualization, and writing–review and editing. Andres De Los Reyes served in a supporting role for conceptualization, investigation, and writing–review and editing. Kathryn A. DeYoung served in a supporting role for data curation, investigation, and writing–review and editing. Jason F. Smith served as lead for formal analysis and served in a supporting role for writing–review and editing. Alexander J. Shackman served as lead for funding acquisition, resources, and supervision and contributed equally to writing–review and editing. Juyoen Hur, Rachael M. Tillman, Jason F. Smith, and Alexander J. Shackman contributed equally to investigation. Rachael M. Tillman, Jason F. Smith, and Alexander J. Shackman contributed equally to conceptualization. Rachael M. Tillman and Jason F. Smith contributed equally to data curation. Rachael M. Tillman and Alexander J. Shackman contributed equally to formal analysis and visualization. Kathryn A. DeYoung and Alexander J. Shackman contributed equally to project administration. Jason F. Smith and Alexander J. Shackman contributed equally to methodology. Juyoen Hur and Alexander J. Shackman contributed equally to writing–original draft.

The data are available at https://osf.io/aj64g/ and https://neurovault.org/collections/15620.

Correspondence concerning this article should be addressed to Juyoen Hur, Department of Psychology, Yonsei University, Room 410, Widang Building, 50 Yonsei-ro Seodaemun-gu, Seoul 03722, Republic of Korea, or Alexander J. Shackman, Department of Psychology, University of Maryland, Biology/Psychology Building, 4094 Campus Drive, College Park, MD 20742, United States. Email: jhur1@yonsei.ac.kr or shackman@umd.edu

uncertain anticipation of potential encounters with social threat. Here we used a novel functional magnetic resonance imaging paradigm to probe the neural circuitry engaged during the anticipation and acute presentation of threatening faces and voices in a racially diverse sample of 66 adolescents selectively recruited to encompass a range of social anxiety and enriched for clinically significant levels of distress and impairment. Results demonstrated that adolescents with more severe social anxiety symptoms experience heightened distress when anticipating encounters with social threat, and reduced discrimination of uncertain social threat and safety in the bed nucleus of the stria terminalis, a key division of the central extended amygdala (EAc). Although the EAc—including the bed nucleus of the stria terminalis and central nucleus of the amygdala—was robustly engaged by the acute presentation of threatening faces and voices, the degree of EAc engagement was unrelated to the severity of social anxiety. Together, these observations provide a neurobiologically grounded framework for conceptualizing adolescent social anxiety and set the stage for the kinds of prospective–longitudinal and mechanistic research that will be necessary to determine causation and, ultimately, to develop improved interventions for this often-debilitating illness.

General Scientific Summary

Clinically significant levels of social anxiety often emerge in adolescence and existing treatments are far from curative for many, underscoring the urgency of developing a deeper understanding of the underlying neurobiology. Leveraging a racially diverse sample of adolescents and a novel brain imaging paradigm, the present results show that more severe social anxiety is associated with diminished discrimination of anticipated social threat and safety in the bed nucleus of the stria terminalis, a brain region thought to play a key role in promoting pathological fear and anxiety. These observations reinforce the hypothesis that alterations in the bed nucleus of the stria terminalis function underlie socially anxious adolescents' maladaptive responses to benign-but-uncertain everyday social encounters—such as anticipating an interaction with a sales associate or asking a routine question in class—and set the stage for targeted replication and extension studies.

Keywords: bed nucleus of the stria terminalis, central extended amygdala, developmental affective neuroscience, developmental psychopathology, pediatric social anxiety

Supplemental materials: https://doi.org/10.1037/abn0000940.supp

Socially anxious individuals are prone to heightened fear, anxiety, and the avoidance of contexts associated with the potential for social scrutiny (D. Beidel et al., 2019). Social anxiety lies on a continuum and, when extreme, can be devastating, with functional impairment evident in many individuals who do not meet full diagnostic criteria (Fehm et al., 2008; Hyett & McEvoy, 2018; Katzelnick et al., 2001; Kessler, 2003; Lipsitz & Schneier, 2000; Merikangas et al., 2002; Schneier et al., 2002). Social anxiety disorder (SAD) is among the most common psychiatric illnesses (lifetime prevalence: ~13%), typically emerges in adolescence, and confers heightened risk for a variety of other developmental, academic, and psychiatric problems, including comorbid internalizing disorders and substance misuse (Angst et al., 2016; Beesdo-Baum & Knappe, 2012; Ernst et al., 2023; Gregory et al., 2007; Hyett & McEvoy, 2018; Jystad et al., 2021; Kessler et al., 2012; Koyuncu et al., 2019; Mathew et al., 2011; Schneier et al., 1992; Stein et al., 2017). Existing treatments are inconsistently effective or associated with significant adverse effects, underscoring the urgency of developing a more complete understanding of the neural systems governing social anxiety in the first decades of life (Batelaan et al., 2017; D. Beidel et al., 2019; Cuijpers et al., 2024; Evans et al., 2021; James et al., 2020; Rapee et al., 2023; Scholten et al., 2013, 2016; Singewald et al., 2023; Spinhoven et al., 2016; Strawn et al., 2021).

Socially anxious adults and youth are prone to elevated distress and arousal in two distinct contexts: (a) when social threat is acute (i.e., certain and imminent), as when performing in front of a group, and (b) when social threat is possible, but uncertain in timing or likelihood, as when first entering a classroom, conversation, or other social environment (APA, 2022; Cain, 2023; Davis et al., 2010; NIMH, 2011). While the underlying neurobiology is undoubtedly complex and multifactorial, converging lines of preclinical research motivate the hypothesis that socially anxious individuals' heighted reactivity to both kinds of threat reflect functional alterations in the central extended amygdala (EAc), a neuroanatomical circuit encompassing the dorsal amygdala in the region of the central nucleus (Ce) and the neighboring bed nucleus of the stria terminalis (BST) (Fox, Oler, Tromp, et al., 2015; Fox & Shackman, 2019; Hur et al., 2019, 2020; Moscarello & Penzo, 2022; Shackman et al., 2024; Shackman & Fox, 2021; Tseng et al., 2023). Both regions are poised to trigger behavioral, psychophysiological, and neuroendocrine responses to threat via dense projections to downstream effector regions (Davis & Whalen, 2001; Fox, Oler, Tromp, et al., 2015). Large-scale neuroimaging studies in monkeys ($n = 238$–592) show that Ce and BST metabolism covaries with trait-like individual differences in freezing, cortisol, and other defensive responses elicited by uncertain naturalistic threats (Fox, Oler, Shackman, et al., 2015; Shackman et al., 2013). Work in humans demonstrates that both regions are sensitive to a broad spectrum of threatening and aversive stimuli (Fox & Shackman, 2019; Hur et al., 2020; Meyer et al., 2019; Murty et al., 2023; Shackman & Fox, 2021). Lesion and other kinds of focal perturbation studies in rodents demonstrate that microcircuits within and between the Ce and BST are critical for orchestrating defensive responses to both acute and uncertain threats (Chen et al., 2022; Fox & Shackman, 2019; Lange et al., 2017; Moscarello & Penzo, 2022; Pomrenze, Giovanetti, et al., 2019; Pomrenze, Tovar-Diaz, et al., 2019; Ren

et al., 2022; Ressler et al., 2020; Zhu et al., 2024), and help calibrate the degree of wariness displayed during interactions with unfamiliar and potentially threatening conspecifics (Lee et al., 2008; Lungwitz et al., 2012; Sajdyk et al., 2008). Although the causal contribution of the BST has yet to be explored in primates, monkeys with fiber-sparing lesions of the Ce show reduced defensive responses to both acute (e.g., snake) and uncertain threat (e.g., human intruder's profile; Kalin et al., 2004; Oler et al., 2016). Complete destruction of the amygdala is associated with reduced signs of anxiety during interactions with unfamiliar animals (Emery et al., 2001). Likewise, humans with circumscribed amygdala damage show atypically low levels of dispositional fear and anxiety—whether indexed by self-report, family report, clinician report, or daily diary—and display a profound lack of fear and anxiety in response to both acute threats (e.g., spiders, snakes, Pavlovian threat cues, and horror movies) and contexts associated with uncertain potential threat (e.g., traversing a haunted house; Bechara et al., 1995; Feinstein et al., 2011, 2016; Korn et al., 2017; Tranel et al., 2006). Conversely, stimulation of the Ce is associated with potentiated responses to uncertain threat in animals and heightened feelings of fear and anxiety in humans, suggesting that circuits centered on this region are necessary and sufficient for many of the core signs and symptoms of social anxiety (Inman et al., 2020; Kalin et al., 2016; Moscarello & Penzo, 2022).

Despite this progress, the relevance of these discoveries to pediatric social anxiety remains unclear. To date, the vast majority of human neuroimaging studies have focused on laboratory analogues of acute social threat, including virtual social interactions and "threat-related" social cues, such as photographs of fearful and angry facial expressions (Jarcho et al., 2013). Meta-analyses show that the EAc is generally hyperreactive to social cues among adults with SAD and those with a childhood history of extreme shyness and behavioral inhibition, key dispositional risk factors for SAD (Brühl et al., 2014; Chavanne & Robinson, 2021; Clauss & Blackford, 2012; Fox & Kalin, 2014; Gentili et al., 2016; Tan et al., 2024). Among adults, EAc reactivity to acute social threat is dampened by clinically effective treatments for SAD, consistent with a causal role (Klumpp & Fitzgerald, 2018; Shackman et al., 2016). While the pediatric social anxiety literature is comparatively sparse, the available evidence suggests a broadly consistent pattern (Jarcho et al., 2013). Nevertheless, some comparatively large-scale studies have failed to detect exaggerated EAc reactivity to acute social threat. For example, Ziv and colleagues reported negligible effects of generalized SAD on amygdala reactivity to dynamically looming hostile faces or film clips of actors delivering social criticism ($n = 67$ unmedicated patients, $n = 28$ matched controls; Ziv et al., 2013).

Much less scientific attention has been devoted to understanding the neural systems underlying heightened reactivity to anticipated social threat. Early work using comparatively low-resolution neuroimaging techniques (e.g., ^{15}O-positron emission tomography) and small case-control designs ($n < 10$/group) revealed evidence of heightened amygdala activity among adults with SAD during the certain anticipation of a speaking challenge (Lorberbaum et al., 2004; Tillfors et al., 2002)—an effect later confirmed in higher resolution studies (3T functional magnetic resonance imaging [fMRI]) and larger samples (Boehme et al., 2014; Davies et al., 2017). Potential group differences in BST activation were neither scrutinized nor reported. More recent work has extended this approach to the uncertain anticipation of social threat (Figel et al., 2019). Here a cue presented at the outset of each trial signaled whether the participant's face would ("threat") or would not ("safety") be video-recorded. Cues were followed by a temporally variable and uncertain anticipation phase (3–16 s) that terminated with the presentation of a second cue indicating whether the camera was recording. Results revealed sustained levels of heightened BST activation in adults with SAD and controls during the uncertain anticipation of social threat encounters. Although patients showed numerically smaller responses, significant group differences were not evident in either the BST or the dorsal amygdala (Ce), and potential regional differences (BST vs. Ce) were not interrogated. While important, the relevance of this body of observations to maladaptive social anxiety earlier in life, during adolescence, remains little explored and largely unknown (but see Michalska et al., 2023 for related efforts in a mixed-anxiety sample of youth).

Here we combined fMRI with a novel threat paradigm—the Maryland Social Threat Countdown (MSTC)—in a racially diverse group of adolescents. The sample was selectively recruited to encompass a broad spectrum of social anxiety—without gaps or discontinuities—and enriched for clinically significant levels of distress and impairment. Adolescent with comorbid anxiety and depressive disorders were enrolled, maximizing clinical relevance (Ernst et al., 2023; Jystad et al., 2021; Koyuncu et al., 2019; Lahey et al., 2022; Tiego et al., 2023). The MSTC task takes the form of a 2 (valence: social threat/safety) × 2 (temporal certainty: uncertain/certain) × 2 (phase: anticipation/presentation) randomized event-related design, allowing us to separately assess EAc activation during the anticipation and acute presentation of both certain and uncertain social-threat cues (Figure 1). On certain social threat trials, participants saw a descending stream of integers ("count-down"). To maximize distress, the anticipation period always culminated with the presentation of a multimodal social threat that included a photograph of an angry young-adult face and an audio clip of a hostile verbal remark (e.g., "no one wants you here"). Uncertain Social Threat trials were similar, but the integer stream was randomized and presented for an unsignaled and variable duration. Here, participants knew that a social threat was coming, but they had no way of knowing precisely when the encounter would occur. Safety trials were similar but terminated with the presentation of normatively benign photographs (happy faces) and audio clips (e.g., "I play soccer").

Anatomically defined regions-of-interest (ROIs) and spatially unsmoothed fMRI data allowed us to rigorously quantify Ce and BST reactivity to the anticipation and presentation of uncertain and certain social threat, and determine whether activation in one or both regions covary with the severity of social anxiety (Figure 1). Unlike voxelwise analyses—which screen thousands of voxels for evidence of statistical significance and yield optimistic effect size estimates in suprathreshold regions—anatomically defined ROIs "fix" the outcomes of interest a priori, providing statistically unbiased estimates of brain-phenotype associations (Poldrack et al., 2017). Exploratory whole-brain voxelwise analyses were also performed, enabling more direct comparison with prior work.

Discovering the neural systems most relevant to adolescent social anxiety is important. It would provide an empirical rationale for prioritizing specific experimental assays (e.g., the uncertain anticipation of social threat) and neurobiological targets (e.g., BST) for prospective–longitudinal and intervention studies in humans (e.g., acute pharmacological challenges, neurofeedback) and mechanistic

Figure 1
Study Overview

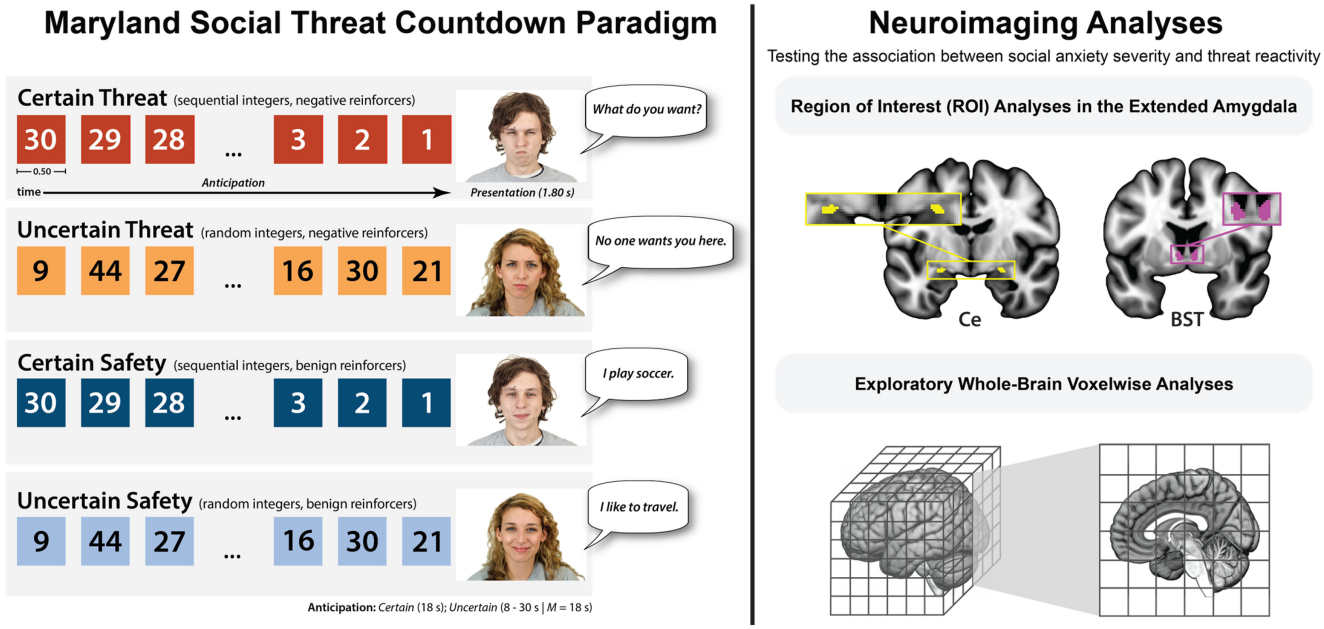

Note. The MSTC paradigm. As shown schematically in the left panel, the MSTC paradigm takes the form of a 2 (valence: social threat/safety) × 2 (temporal certainty: uncertain/certain) × 2 (phase: anticipation/presentation) repeated-measures randomized event-related design. On certain social threat trials, participants saw a descending stream of integers ("count-down") for 18 s. To maximize distress, the anticipation epoch always culminated with the presentation of a multimodal social threat (1.8 s), encompassing a photograph of an angry face and an audio clip of a hostile verbal remark (e.g., "no one wants you here"). Uncertain social threat trials were similar, but the integer stream was randomized and presented for an uncertain and variable duration (8–30 s; $M = 18$ s). Participants knew that a social threat would occur, but they had no way of knowing precisely when the encounter would occur. Safety trials were similar but terminated with the delivery of normatively benign photographs (happy faces) and audio clips (e.g., "I play soccer"). Neuroimaging analyses. As shown schematically in the top-right panel, two analytic approaches were used to determine the impact of social anxiety on neural reactivity to social threat. Hypothesis testing focused on two well-established, anatomically defined EAc ROIs: the Ce is marked in yellow (light gray); the BST is marked in magenta (dark gray). Because the ROIs (i.e., voxel-level measurements) were chosen a priori—on the basis of neuroanatomy, rather than suprathreshold activation—this approach provides statistically unbiased effect-size estimates (Poldrack et al., 2017). Standardized regression coefficients were extracted and averaged across voxels for each combination of ROI, condition, and participant. Hypothesis testing used a standard GLM. For illustrative purposes, 1-mm ROIs are shown. Analyses employed ROIs decimated to the 2-mm resolution of the fMRI data. As shown schematically in the bottom-right panel, exploratory whole-brain voxelwise analyses were also performed. ROI = region of interest; Ce = central nucleus of the amygdala; BST = bed nucleus of the stria terminalis; MSTC = Maryland Social Threat Countdown; EAc = central extended amygdala; GLM = general linear model; fMRI = functional magnetic resonance imaging. Facial stimuli are from the Chicago Face Database. See "The Chicago Face Database: A Free Stimulus Set of Faces and Norming Data," by D. S. Ma, J. Correll, and B. Wittenbrink, 2015, *Behavior Research Methods*, *47*(4), pp. 1122–1135 (https://doi.org/10.3758/s13428-014-0532-5). CC BY 4.0. Reprinted with permission. See the online article for the color version of this figure.

studies in animals. Animal models are critical for identifying the molecules and microcircuits that underlie aberrant EAc threat processing and, ultimately, for developing novel pharmacological treatments for this often-debilitating disorder (Fox & Shackman, 2019).

Method

Recruitment and Study Overview

Adolescents (13–17 years) were recruited using a multipronged strategy, including online advertisements (e.g., Facebook, parent listservs), flyers posted at community mental health clinics and other high-traffic community settings (e.g., coffee shops, libraries, community centers), and referrals from ongoing research studies. To capture a broad spectrum of social anxiety, with substantial enrichment for elevated levels of distress and impairment, separate advertisements were used to target adolescents with elevated (e.g., shy teens) and low-to-middling symptoms. Following preliminary screening, potentially eligible individuals completed a single face-to-face session that included a self-report assessment, a structured clinical interview, and a magnetic resonance imaging (MRI) assessment. Guardians and adolescents provided informed written consent and assent, respectively. All procedures were approved by the University of Maryland Institutional Review Board (Protocol 661215). The study design, hypotheses, and analytic strategy were not preregistered.

Participants and Eligibility Criteria

Potentially interested adolescents completed an online screening assessment, including the abbreviated Social Phobia and Anxiety Scale for Children-11 (SPAIC-11), which quantifies the frequency of social-anxiety symptoms across different social settings (Bunnell et al., 2015). Three additional ad hoc items (How much does anxiety bother you or cause you distress? How much does anxiety "mess

things up" for you? How much of an effect does anxiety have on your life?) were added to the screening assessment shortly after enrollment began and were used to probe the degree of distress and impairment on a 5-point Likert scale ranging from 1 (*not at all*) to 5 (*extremely*). Adolescents were invited to enroll if, at the time of the preliminary screening, they showed evidence of either (a) significant social anxiety, as indexed by an abbreviated SPAIC-11 score of >15 or moderate-to-severe (≥3) distress/impairment on one or more of the three follow-up items; or (b) middling-to-low social anxiety, as indexed by an abbreviated SPAIC-11 score of <7 and, if available, little-to-no (<3) distress/impairment on the three additional items.

All participants and their caregivers indicated that they were right-handed, native English speakers, with a full-term pregnancy (>34 weeks) and normal or corrected-to-normal color vision. Participants reported that they were free from psychiatric medications; standard MRI contraindications; and a lifetime history of severe head injury, neurological signs and disorders, psychotic disorders, and developmental delays or disorders (e.g., autism).

In total, 78 adolescents and their caregivers participated. Twelve participants were excluded from analyses due to premature termination of the MRI assessment ($n = 3$), inadequate compliance with the in-scanner rating task (<50% ratings completed; $n = 3$), or insufficient usable data ($n = 6$; see below for details). The final sample included 66 adolescents ($M = 15.4$ years, $SD = 1.3$; 60.6% female; 50.0% White, 30.3% African American/Black, 7.6% Hispanic, 6.1% Asian, 6.1% multiracial/other). The sample showed a broad spectrum of social anxiety (SPAIC: $M = 10.0$, $SD = 6.0$, range = 0.0–21.3). Half of the sample ($n = 33$, 60.6% female) met the SPAIC-11 cutoff (>9.17) for probable SAD (Bunnell et al., 2015). The sample was significantly enriched for SAD diagnoses according to the *Diagnostic and Statistical Manual of Mental Disorders*, fourth edition ($n = 24$, 58.3% female). As expected, comorbidity was rampant, and the majority of adolescents with SAD ($n = 14$, 58.3%) received at least one other categorical diagnosis (Koyuncu et al., 2019; Lahey et al., 2022; Tiego et al., 2023). Generalized anxiety disorder ($n = 12$, 50.0%) and major depressive disorder ($n = 8$, 33.3%) were the most common comorbidities, in broad accord with recent adolescent epidemiology studies (Ernst et al., 2023; Jystad et al., 2021).

Clinical Assessments

Abbreviated SPAIC-11

Consistent with recent methodological recommendations, the 11-item SPAIC was used to quantify dimensional variation in adolescent-reported social anxiety (Bunnell et al., 2015; Tulbure et al., 2012; Wong et al., 2016). Prior work demonstrates that the SPAIC is reliable, sensitive to *Diagnostic and Statistical Manual of Mental Disorders* diagnostic status, responsive to treatment, and correlated with independent assessments of social anxiety, including parent report and speech latency during a public-speaking challenge (D. C. Beidel et al., 2000; Bunnell et al., 2015; Tulbure et al., 2012; Wong et al., 2016). Each of the 11 items probe the frequency of fear or anxiety evoked by a specific, developmentally appropriate social situation (e.g., "…feel scared when I have to speak or read in front of a group of people"), using a 3-point Likert scale ranging from 0 (*never*) to 2 (*always*). Ten of the 11 items focus on subjective symptoms of fear and anxiety ("feel scared"), whereas the remaining item focuses on a behavioral sign ("…do not speak to anyone until they speak to me"). Eight of the items (e.g., "…feel scared when I start to talk to…") required separate responses for different types of interaction partners (boys or girls my age that I know, boys or girls my age that I do not know, adults; D. C. Beidel et al., 1995). Responses for these items were averaged across partners and rounded to the nearest integer (Bunnell et al., 2015). Higher scores indicate more pervasive and severe social anxiety (D. C. Beidel et al., 2000). In the present sample, total SPAIC-11 sum scores showed acceptable reliability ($\alpha = .94$), were strongly correlated with SAD diagnostic status ($r = .66$), and were independent of age and biological sex ($|r| < .16$). As expected, based on the observed pattern of diagnostic comorbidity (see above), total SPAIC-11 scores were associated with the presence of other internalizing diagnoses (e.g., generalized anxiety disorder: $r = .50$).

Mini-International Neuropsychiatric Interview (MINI) for Children and Adolescents

For descriptive purposes, diagnostic status was assessed by a masters-level clinician using the MINI for children and adolescents (Sheehan et al., 2010). To encourage frank reporting, diagnostic interviews were completed without the caregiver present.

MSTC Paradigm

Task Structure

Building on prior work in adults (Grogans et al., 2024; Hur et al., 2020, 2022; Kim et al., 2023), the MSTC paradigm takes the form of a 2 (valence: social threat/safety) × 2 (temporal certainty: uncertain/certain) × 2 (phase: anticipation/presentation) repeated-measures, randomized event-related design (Figure 1). On certain social threat trials, participants saw a descending stream of integers ("countdown") for 18 s. To maximize distress, the anticipation period always culminated with the presentation of a multimodal social threat (1.8 s) encompassing a photograph of an angry young-adult face and an audio clip of a hostile verbal remark (e.g., "No one wants you here"). Uncertain social threat trials were similar, but the integer stream was randomized and presented for a temporally uncertain and variable duration (range = 8–30 s; $M = 18$ s). On uncertain trials, integers were randomly drawn from a near-uniform distribution ranging from 1 to 45 to reinforce the impression that uncertain trials could be much longer than certain ones and to minimize incidental temporal learning ("time-keeping"). White-noise visual masks (3.2 s) were presented between trials to minimize persistence of the visual reinforcers in iconic memory. Safety trials were similar but terminated with the delivery of normatively benign photographs (happy faces) and audio clips ("I play soccer"). Consistent with recent recommendations (Shackman & Fox, 2016), the mean duration of the anticipation phase was identical across conditions, ensuring an equal number of measurements (i.e., repetition times [RT] per condition). Mean duration was chosen to enhance detection of task-related differences in the blood oxygen level-dependent signal (Henson, 2007). Valence was continuously signaled throughout the anticipation epoch by the background color of the display. Certainty was signaled by the nature of the integer stream. Participants were periodically prompted (following the offset of the visual mask) to rate the intensity of fear/anxiety experienced a few moments earlier, during the anticipation period of the prior

trial, using a 1–4 (*least/most*) scale and an MRI-compatible response pad (MRA, Washington, Pennsylvania, United States). Participants rated each trial type once per scan (16.7% trials). Participants were completely informed about the task design and contingencies prior to scanning. The task was administered in three scans, with short breaks between scans. Simulations were used to optimize the trial order and timing to minimize predictor collinearity (variance inflation factors < 1.68) (Mumford et al., 2015). Stimulus presentation and ratings acquisition were controlled using presentation software (Version 19.0, Neurobehavioral Systems, Berkeley, California, United States).

Procedures

Prior to fMRI scanning, participants practiced an abbreviated version of the paradigm until participants indicated and staff confirmed understanding. During scanning, foam inserts were used to immobilize the participant's head within the head-coil and mitigate potential motion artifact. Participants were continuously monitored using an MRI-compatible eye-tracker (Eyelink 1000; SR Research, Ottawa, Ontario, Canada) and the AFNI real-time motion plugin (Cox, 1996). Eye-tracking data were not recorded. Measures of respiration and breathing were continuously acquired during scanning using a Siemens respiration belt and photoplethysmograph affixed to the first digit of the non-dominant hand. Following the last scan, participants were removed from the scanner, debriefed, compensated, and discharged.

Visual Stimuli

A total of 72 face photographs were drawn from the Chicago Face Database (Versions 1–2) (Ma et al., 2015). Stimuli included 36 young-adult models of varying race and sex, each depicting one angry and one happy expression. Visual stimuli were digitally back-projected onto a semiopaque screen mounted at the head-end of the scanner bore and viewed using a mirror mounted on the head-coil (Powerlite Pro G5550, Epson America, Inc., Long Beach, California, United States).

Auditory Stimuli

A total of 72 custom auditory stimuli were created by recording 36 young-adult voice actors, recruited to match the apparent sex and race of the photograph models. Each voice actor provided one threatening and one benign audio statement, equated for the number of syllables. Voice actors were carefully coached to deliver the threatening statements (e.g., "I don't like you") in a hostile manner and to deliver the benign statements (e.g., "Today is nice") in a neutral or mildly positive manner. Audio stimuli were volume standardized. To reinforce the naturalistic nature of the paradigm, each photograph was consistently paired with a specific sex- and race-matched voice actor. Auditory stimuli were delivered using an amplifier (PA-1 Whirlwind) with in-line noise-reducing filters and ear buds (S14; Sensimetrics, Gloucester, Massachusetts, United States) fitted with noise-reducing ear plugs (Hearing Components, Inc., St. Paul, Minnesota, United States).

MRI Data Acquisition

MRI data were acquired using a Siemens Magnetom 3T Tim Trio system (32-channel head-coil). Sagittal T1-weighted anatomical images were acquired using a magnetization prepared rapid acquisition gradient echo sequence (RT = 1,900 ms; TE = 2.32 ms; inversion = 900 ms; flip = 9°; sagittal slice thickness = 0.9 mm; in-plane = 0.449 × 0.449 mm; matrix = 512 × 512; field-of-view = 230 × 230). To enhance anatomical resolution, a multiband sequence was used to collect oblique-axial echo planar imaging (EPI) volumes during the MSTC task (multiband acceleration = 6; RT = 1,000 ms; TE = 39.4 ms; flip = 36.4°; slice thickness = 2.2 mm, number of slices = 66; in-plane = 2.1875 × 2.1875mm; matrix = 96 × 96). Images were collected in the oblique-axial plane (approximately −20° relative to the anterior and posterior commissure plane) to minimize potential susceptibility artifacts. A total of three 568-volume scans were acquired. The scanner automatically discarded seven volumes prior to the first recorded volume. To enable field map distortion correction, a pair of oblique-axial coplanar spin echo images with opposing phase encoding direction was also acquired (RT = 7,220 ms; TE = 73 ms; slice thickness = 2.2 mm; matrix = 96 × 96).

MRI Data Pipeline

Methods were optimized to minimize spatial-normalization error and other potential sources of noise. Data were visually inspected before and after processing for quality assurance.

Anatomical Data Processing

Methods are similar to those described in other recent reports by our group (Grogans et al., 2024; Hur et al., 2018, 2020, 2022; Kim et al., 2023). T1-weighted images were inhomogeneity corrected using N4 (Tustison et al., 2010) and denoised using ANTS (Avants et al., 2011). The brain was then extracted using BEaST (Eskildsen et al., 2012) and brain-extracted and normalized reference brains from IXI (BIAC, 2022). Brain-extracted T1 images were normalized to a version of the brain-extracted 1-mm T1-weighted MNI152 (Version 6) template (Grabner et al., 2006) modified to remove extracerebral tissue. Normalization was performed using the diffeomorphic approach implemented in SyN (Version 2.3.4; Avants et al., 2011). Brain-extracted T1 images were segmented—using native-space priors generated in FAST (Version 6.0.4; Jenkinson et al., 2012)—to enable T1-EPI coregistration (see below).

Fieldmap Data Processing

Standard error images and topup were used to create fieldmaps. Fieldmaps were converted to radians, median-filtered, and smoothed (2 mm). The average of the distortion-corrected standard error images was inhomogeneity corrected using N4 and masked to remove extracerebral voxels using 3dSkullStrip (Version 19.1.00).

Functional Data Processing

EPI files were despiked using 3dDespike, slice-time corrected to the RT center using 3dTshift, and motion corrected to the first volume and inhomogeneity corrected using ANTS (12-parameter affine). Transformations were saved in ITK-compatible format for subsequent use (McCormick et al., 2014). The first volume was extracted for T1-EPI coregistration. The reference EPI volume was simultaneously coregistered with the corresponding T1-weighted image in native space and corrected for geometric distortions

using boundary-based registration (Jenkinson et al., 2012). This step incorporated the previously created fieldmap, undistorted standard error, T1, white matter (WM) image, and masks. The spatial transformations necessary to transform each EPI volume from native space to the reference EPI, from the reference EPI to the T1, and from the T1 to the template were concatenated and applied to the processed EPI data in a single step to minimize incidental spatial blurring. Normalized EPI data were resampled (2 mm^3) using fifth-order b-splines. To maximize anatomical resolution, no additional spatial filters were applied, consistent with recent recommendations (Tillman et al., 2018) and other work by our group (Grogans et al., 2024; Kim et al., 2023). Hypothesis testing focused on anatomically defined ROIs (see below). By convention, exploratory whole-brain voxelwise analyses employed data that were spatially smoothed (6 mm; 3DblurInMask).

fMRI Data Exclusions and Modeling

Data Exclusions

Participants who responded to <50% of rating prompts—indicating inadequate task engagement—were excluded from analyses ($n = 3$). Volume-to-volume displacement (>0.5 mm) was used to assess residual motion artifact. Scans with excessively frequent artifacts (≥2.5 *SD*) were discarded. To assess task-correlated motion, we computed correlations between the design matrix and motion estimates (see above). Scans showing extreme correlations (≥ 2.5 *SD*) were discarded. Participants who failed to provide at least two scans of usable data were censored from analyses ($n = 6$).

Canonical First-Level Modeling

For each participant, first-level modeling was performed using standard general linear models (GLMs) implemented in SPM12 (Version 7771), with the default autoregressive model and the temporal band-pass filter set to the hemodynamic response function (HRF) and 128 s (Wellcome Centre for Human Neuroimaging, 2022). Anticipatory hemodynamic signals were modeled using variable-duration rectangular ("boxcar") regressors spanning the anticipation ("countdown") epochs of the uncertain threat, certain threat, and uncertain safety trials; and convolved with a canonical HRF and its temporal derivative. To maximize design efficiency, certain-safety anticipation served as the reference condition and contributed to the baseline estimate (Poline et al., 2007). Epochs corresponding to the acute presentation of threatening and benign face/voice stimuli were simultaneously modeled using the same approach, separately for each of the four trial types (Figure 1). Epochs corresponding to the presentation of the white-noise visual masks and rating prompts were treated as nuisance regressors. EPI volumes acquired before the first trial and following the final trial were unmodeled and contributed to the baseline estimate. Consistent with prior work using shock-reinforced variants of the countdown task in adults (Grogans et al., 2024; Hur et al., 2020, 2022; Kim et al., 2023), additional nuisance variates included estimates of volume-to-volume displacement, motion (six parameters, 0- and 1-volume lagged), cerebrospinal fluid (CSF) signal, instantaneous pulse and respiration rates, and ICA-derived nuisance signals (e.g., brain edge, CSF edge, global motion, and WM; Pruim et al., 2015). Volumes with excessive volume-to-volume displacement (>0.33 mm) were censored.

Extended Amygdala Regions of Interest (ROIs)

Consistent with prior work by our group, task-related Ce and BST activation was quantified using well-established, anatomically defined ROIs and spatially unsmoothed fMRI data (Grogans et al., 2024; Hur et al., 2018; Kim et al., 2023; Figure 1). The derivation of the Ce ROI is detailed in Tillman et al. (2018). The probabilistic BST ROI was developed by Theiss and colleagues and thresholded at 25% (Theiss et al., 2017). The BST ROI mostly encompasses the supracommissural BST, given the difficulty of reliably discriminating the borders of regions below the anterior commissure in T1-weighted MRIs (Krüger et al., 2015). Bilateral ROIs were decimated to the 2-mm resolution of the fMRI data. EAc ROI analyses used standardized regression coefficients extracted and averaged for each combination of task contrast (e.g., uncertain threat vs. certain safety anticipation), ROI, and participant.

Analytic Strategy

Overview

The overarching goal of this study was to determine the impact of variation in social anxiety (*z*-transformed SPAIC-11) on reactivity to the MSTC paradigm (Figure 1). Hypothesis testing focused on two measurement modalities: (a) in-scanner ratings of anticipatory distress and (b) fMRI measures of EAc (Ce/BST) activation during the anticipation and presentation phases of the MSTC paradigm. Except where otherwise noted, analyses were performed using SPSS (Version 27.0.1). Diagnostic procedures (e.g., influence statistics) and data visualizations were used to confirm test assumptions (Tukey, 1977). Predictor collinearity was acceptable for all analytic models. Some figures were created using R (Version 4.0.2), RStudio, and ggplot2 (Version 3.4.1) (R Core Team, 2022; RStudio Team, 2022; Wickham, 2016).

Behavioral Hypothesis Testing

A standard mixed-effects GLM was used to determine whether the anticipation of social threat elicits distress, test whether individual differences in social anxiety are associated with amplified distress, and explore the possibility that these effects are conditional on the temporal certainty of social encounters. Paralleling the MSTC paradigm, the GLM was implemented as a 2 (valence: social threat/safety) × 2 (temporal certainty: uncertain/certain) design with social anxiety (*z*-transformed SPAIC-11) included as a dimensional predictor. In effect, this model allowed us to partition variance in anticipatory distress into that associated with the experimental task, with the severity of social anxiety, and with their interaction. Significant effects were interrogated using focal contrasts (paired Students *t* tests) and regressions as appropriate. Hotelling's *t* test, as implemented in Fisher's Z transform (Garbin, 2024), was used to compare dependent correlations (Hotelling, 1940).

fMRI Hypothesis Testing

Standard mixed-effects GLMs were used to probe the association between standardized social anxiety symptoms and EAc (Ce/BST)

reactivity to the anticipation and presentation of social threat, and to explore the possibility that these effects are conditional on the temporal certainty of threat encounters. For the anticipation phase, the GLM was implemented as a 3 (condition: uncertain social threat, certain social threat, and uncertain safety) × 2 (region: Ce, BST) design with social anxiety (*z*-transformed SPAIC-11) included as a dimensional predictor. This analytic choice was dictated by the fact that the anticipation phase of certain safety trials served as the implicit baseline condition for first-level fMRI models (see above). Huynh–Feldt correction was used as necessary. For the presentation phase, the GLM was implemented as a 2 (valence: social threat, safety) × 2 (temporal certainty: uncertain, certain) × 2 (region: Ce, BST) design with social anxiety again included as a dimensional predictor. For both GLMs, significant interactions were again decomposed using focal contrasts (paired students *t* tests) and regressions.

In head-to-head comparisons of criterion validity, simple paper-and-pencil measures often outperform more sophisticated brain imaging metrics (Shackman & Fox, 2018). To gauge the added explanatory value ("incremental validity") of statistically significant brain metrics, we recomputed the relevant multiple regressions while simultaneously incorporating paper-and-pencil distress ratings or *z*-transformed SAD diagnostic status. Sensitivity analyses confirmed that key conclusions were minimally altered by the inclusion of nuisance variation in biological sex, pubertal status (Petersen et al., 1988), or age (not reported).

Results

The Anticipation of Social Threat Elicits Distress

As shown in Figure 2a, in-scanner ratings of fearful and anxious distress were elevated during the anticipation of social threat compared to safety, and during the anticipation of temporally uncertain compared to certain social cues—valence: $F(1, 64) = 47.39$, $p < .001$, $\eta_p^2 = .43$; certainty: $F(1, 64) = 18.18$, $p < .001$, $\eta_p^2 = .22$. These observations dovetail with work focused on threat-of-shock paradigms in adults and reinforce the validity of the MSTC paradigm for probing social anxiety in adolescents (Grogans et al., 2024; Hur et al., 2020; Kim et al., 2023).

Social Anxiety Potentiates Distress During the Anticipation of Social Threat

As shown in Figure 2b, adolescents with more severe social anxiety reported heightened distress during the anticipation of social threat relative to safety—Valence × Social Anxiety: $F(1, 64) = 7.81$, $p = .01$, $\eta_p^2 = .11$. Although the main effect of social anxiety was also significant, $F(1, 64) = 4.80$, $p = .03$, $\eta_p^2 = .07$, follow-up tests showed that this was entirely driven by the association with threat-elicited distress—threat: $t(64) = 2.79$, $p = .007$; safety: $t(64) = 1.01$, $p = .32$; threat-versus-safety: $t_{\text{hoteling}}(63) = 2.20$, $p = .03$. Likewise, in a simultaneous regression model, only threat-related distress was significantly and uniquely associated with dimensional variation in social anxiety—threat: $t(63) = 2.85$, $p = .006$; safety: $t(63) = -1.21$, $p = .23$.

The EAc Is Preferentially Engaged by the Anticipation of Uncertain Social Threat

We used anatomically defined Ce and BST ROIs and spatially unsmoothed fMRI data to test whether more severe social anxiety symptoms are associated with amplified EAc activation when anticipating social-threat encounters, and to explore the possibility that the degree of amplification depends on the temporal certainty of encounters. A mixed-effects GLM revealed a significant effect of Region, reflecting greater activation, on average, in the Ce compared to the BST, $F(1, 64) = 4.81$, $p = .03$, $\eta_p^2 = 0.07$. The condition effect was also significant, $F(2, 128) = 3.84$, $p = .02$, $\eta_p^2 = .06$. As shown in Figure 3a, the anticipation of uncertain

Figure 2

In-Scanner Ratings of Subjective Distress

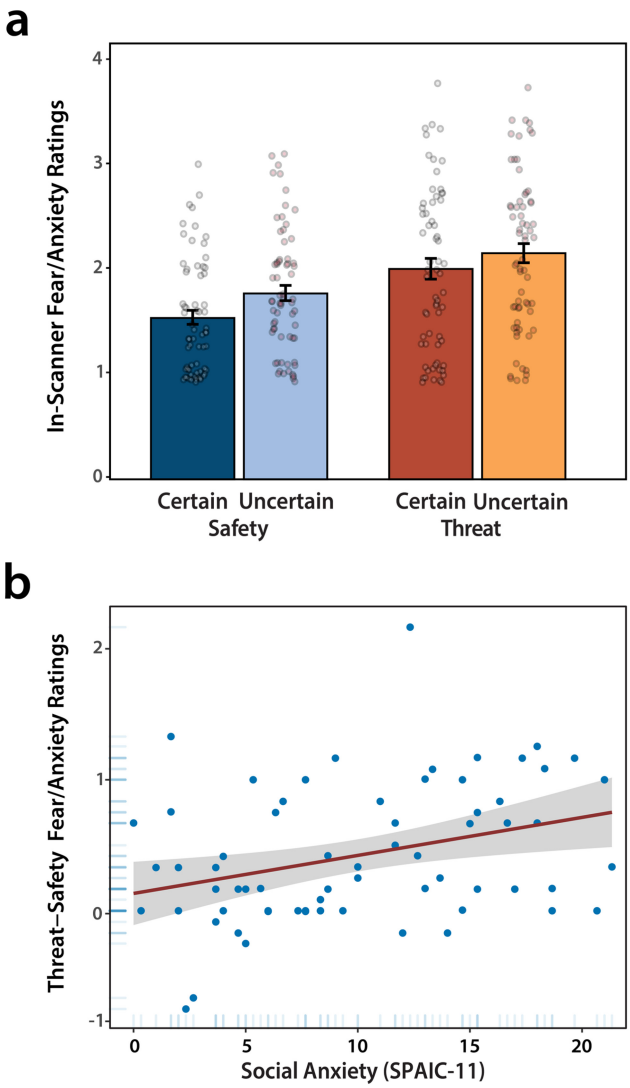

Note. (a) Fear and anxiety were significantly elevated during the anticipation of social threat compared to safety, and during the anticipation of temporally uncertain compared to certain reinforcers ($p < .001$). Error bars depict the standard error of the mean. Dots indicate individual participants. (b) More anxious adolescents experience heightened distress during the anticipation of threatening, compared to benign, social cues ($p = .01$). The line depicts the regression slope. Gray envelope depicts the 95% confidence interval. Dots indicate individual participants. SPAIC-11 = Social Phobia and Anxiety Scale for Children-11. See the online article for the color version of this figure.

Figure 3

Anticipation Phase of the Maryland Social Threat Countdown Paradigm

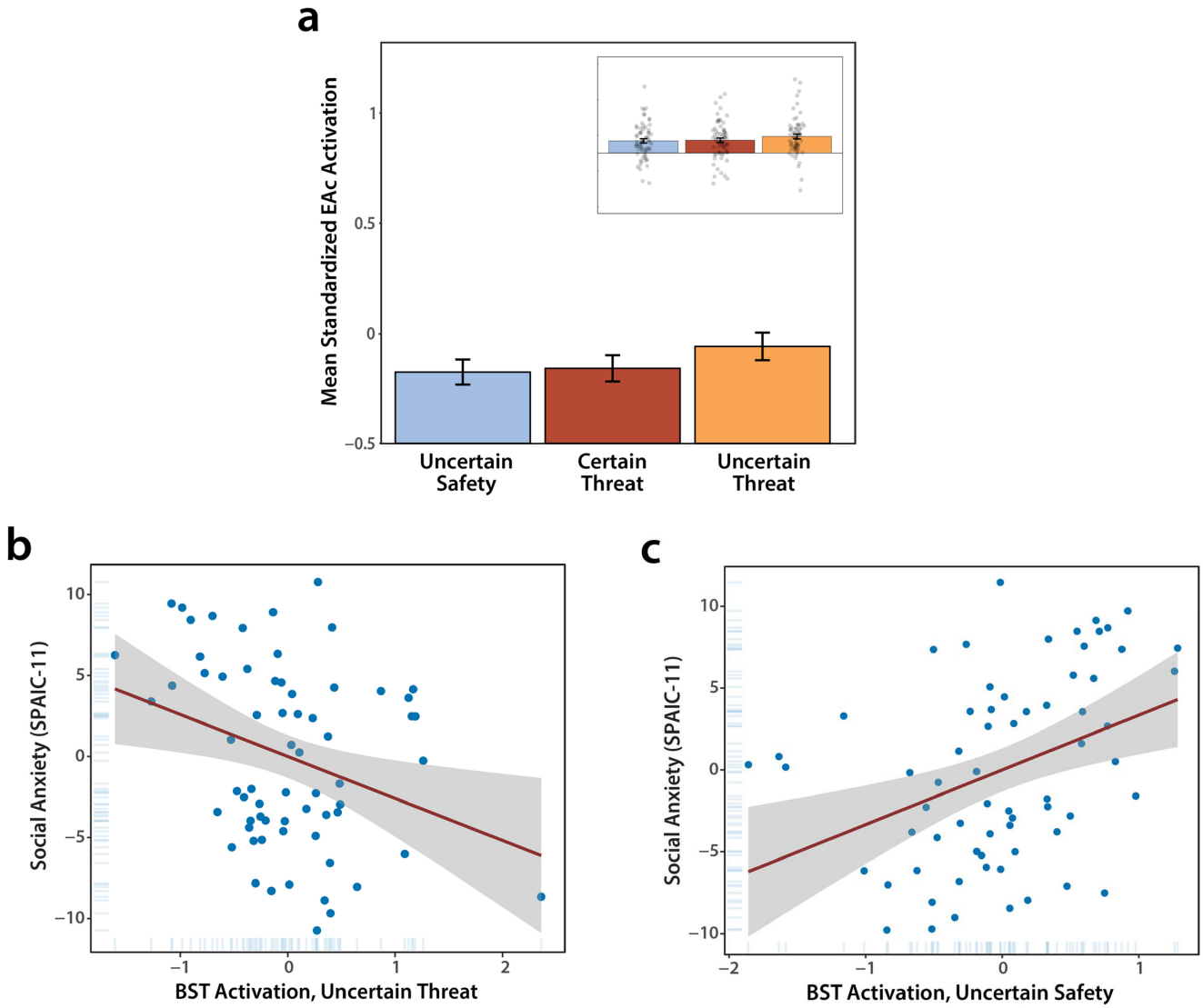

Note. (a) The EAc is preferentially engaged by the temporally uncertain anticipation of social threat ($p = .03$). Inset depicts individual participants. Error bars depict the standard error of the mean. (b) Adolescents with more severe social anxiety show diminished BST reactivity during the temporally uncertain anticipation of social threat, while controlling for differences in Ce anticipatory activation ($p = .01$). (c). Socially anxious adolescents show amplified BST reactivity during the temporally uncertain anticipation of normatively benign social stimuli, while controlling for differences in Ce anticipatory activation ($p = .002$). Conventions are identical to Figure 2. EAc = central extended amygdala; SPAIC-11 = Social Phobia and Anxiety Scale for Children-11; BST = bed nucleus of the stria terminalis; Ce = central nucleus of the amygdala. See the online article for the color version of this figure.

social threat elicited greater EAc activation (averaged across regions) compared to both certain social threat and uncertain safety—certain threat: $t(64) = 2.56$, $p = .01$; uncertain safety: $t(64) = 2.07$, $p = .04$—which in turn did not significantly differ from one another, $t(64) = -0.39$, $p = .70$. The Condition × Region interaction was not significant ($p = .57$). Together, these results indicate that the EAc is preferentially engaged by the anticipation of uncertain social threat—consistent with prior work in adults (Figel et al., 2019)—but the degree of engagement does not appreciably differ across the Ce and BST, its two major divisions.

Social Anxiety Is Associated With Diminished BST Discrimination of Anticipated Threat and Safety

The GLM also revealed significant Condition × Social Anxiety, $F(2, 128) = 5.87$, $p = .004$, $\eta_p^2 = .08$, and Condition × Region × Social Anxiety interactions, $F(2, 128) = 4.75$, $p = .01$, $\eta_p^2 = .07$. Other effects were not significant ($p > .46$). To decompose the significant three-way interaction, we computed separate regression models for the Ce and BST, in each case including reactivity to each of the three anticipation conditions—uncertain social threat, certain social threat, and uncertain safety—as simultaneous predictors of social

anxiety. Results indicated that Ce activation is unrelated to variation in social anxiety, $|t|(62) < 1.19$, $p > .23$. On the other hand, blunted BST reactivity to uncertain-threat anticipation and heightened BST reactivity to uncertain-safety anticipation were both associated with more severe social anxiety—uncertain threat: $t(62) = -2.52$, $p = .01$; uncertain safety: $t(62) = 2.34$, $p = .02$, with negligible effects evident for certain-threat anticipation, $t(62) = 0.17$, $p = .87$. As shown in Figure 3b and 3c, both associations remained significant while controlling for variation in Ce activation, indicating a statistically unique association between BST reactivity and the severity of adolescent social anxiety—uncertain threat: $t(60) = -2.57$, $p = .01$; uncertain safety: $t(60) = 3.23$, $p = .002$.

These results demonstrate that the most robust EAc activation occurs during the uncertain anticipation of social threat, with significantly lower activation evident during the uncertain anticipation of encounters with normatively safe social cues (Figure 3a). This suggests that the normative mean difference across the two conditions is diminished in the BST of adolescents with more severe social anxiety. Consistent with this intuition, higher social anxiety was negatively associated with the simple arithmetic difference in BST activation across the two conditions—uncertain social threat–uncertain safety, anticipation: $r(64) = -.38$, 95% CI [.15, .57], $p = .002$. Although exploratory voxelwise analyses revealed a number of regions that were recruited during social-threat anticipation, they uncovered no whole-brain significant associations with social anxiety (Supplemental Tables S1–S7).

To clarify the explanatory value of BST reactivity, we computed a new regression model, using a combination of the BST neuroimaging metrics and two self-report metrics acquired during the MSTC—indiscriminate distress (Threat + Safety Ratings) and threat-potentiated distress (Threat − Safety Ratings)—to predict social anxiety (cf., Figure 2). Results indicated that BST activation during the anticipation of uncertain threat and safety continued to explain significant variance in social anxiety while controlling for both forms of task-related distress—uncertain threat: $t(61) = -2.85$, $p = .006$; uncertain safety: $t(61) = 2.86$, $p = .006$; ratings: $t(61) < 1.48$, $p > .14$. The same conclusion was also evident using the difference in anticipatory BST activation across the two conditions, $t(62) = -2.76$, $p = .008$ or when controlling for all four condition-specific distress ratings, $|t|(59) > 2.23$, $p < .03$. The difference in anticipatory BST activation also explained significant variance in the severity of social anxiety while controlling for SAD diagnostic status, $t(62) = -2.62$, $p = .01$. In short, BST anticipatory activation explains dimensional variation in adolescent social anxiety above-and-beyond that accounted for by more traditional self- and clinician-assessments, underscoring the added value ("incremental validity") of the fMRI metrics. These observations also make it clear that the association between indiscriminate BST anticipatory activation and social anxiety cannot be attributed to simple differences in subjective reactivity to the MSTC paradigm.

The EAc Is Robustly Recruited by the Presentation of Social Threat, Independent of Social Anxiety

As shown in Figure 4, a mixed-effects GLM indicated that the EAc (Ce and BST) was more strongly engaged by the presentation of threatening compared to normatively benign faces and voices—valence: $F(1, 64) = 8.03$, $p = .006$, $\eta_p^2 = .11$. Results also demonstrated that the Ce was more responsive to the acute presentation of social cues—irrespective of their valence—when compared to the BST—region: $F(1, 64) = 11.56$, $p = .001$, $\eta_p^2 = .15$. No other effects were significant ($p > .18$). In sum, while the EAc, in aggregate, is robustly recruited by the acute presentation of threatening face-voice stimuli, this is largely independent of variation in the severity of social anxiety symptoms.

Figure 4

Presentation Phase of the Maryland Social Threat Countdown Paradigm

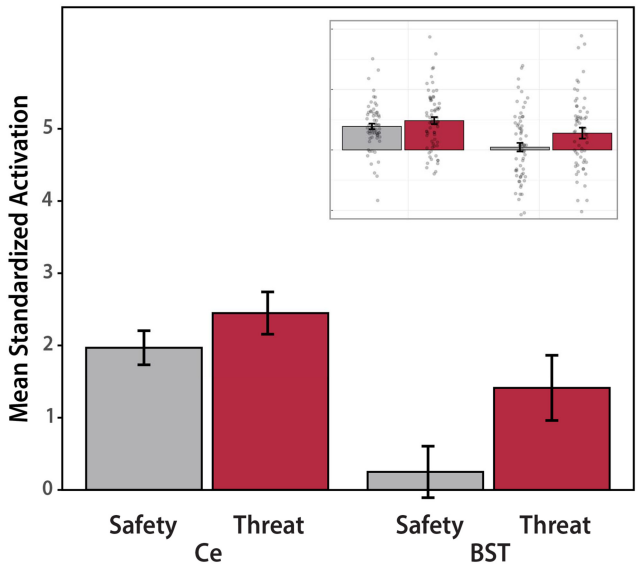

Note. GLM results demonstrated that the EAc was more strongly recruited by the acute presentation of threatening (relative to benign) social stimuli ($p = .006$) and that the Ce is more responsive (relative to the BST) to faces and voices, irrespective of their valence ($p = .001$). Inset depicts individual participants. Other conventions are identical to Figure 2. Ce = central nucleus of the amygdala; BST = bed nucleus of the stria terminalis; GLM = general linear model; EAc = central extended amygdala. See the online article for the color version of this figure.

As expected, a whole-brain voxelwise analysis confirmed that the presentation of faces and voices recruited the amygdala and relevant areas of sensory cortex, including the bilateral fusiform gyri, superior temporal sulci, and Heschl's gyri (Tables S8–S10 in the online supplemental materials). Exploratory analyses did not detect any whole-brain significant voxelwise associations with dimensional variation in social anxiety (Tables S11–S22 in the online supplemental materials).

Discussion

Among socially anxious adolescents, distress and impairment can be triggered by both acute social scrutiny, such as interacting with unfamiliar peers, and settings where negative evaluations are possible, but uncertain in their timing or likelihood, as when first entering a public restroom or navigating a school hallway. To date, comparatively little scientific attention has been devoted to understanding the neural systems underlying heightened reactivity to anticipated social threat. Here we leveraged a novel fMRI paradigm—the MSTC task—in a racially diverse sample of adolescents selectively recruited to encompass a broad spectrum of social anxiety symptoms (50% adolescents of color; 50.0% positive SAD screen; 36.4%

SAD diagnosis) (Figure 1). Results demonstrated that fearful and anxious feelings were significantly elevated, on average, during the anticipation of threatening social cues, confirming the basic validity of the MSTC task as a probe of social anxiety (Figure 2a). Adolescents with more severe social anxiety reported potentiated distress when anticipating encounters with social threat (Figure 2b). Neuroimaging results revealed robust EAc (Ce and BST) activation during the uncertain anticipation of social threat, relative to the anticipation of both certain threat and uncertain safety (Figure 3a). Adolescents with more severe social anxiety showed blunted BST activation during the uncertain anticipation of social threat and heightened BST activation during the uncertain anticipation of benign social cues, indicating diminished discrimination of the two contexts. Indeed, follow-up analyses demonstrated that more severe symptoms were also associated with a reduction in the difference in BST activation across the two conditions. These brain-anxiety associations remained significant when controlling for Ce reactivity, paper-and-pencil measures of task-related distress, or SAD diagnostic status, underscoring the unique explanatory value of BST anticipatory activity (Figure 3b and 3c). Although the EAc (Ce and BST) was robustly engaged during the acute presentation of threatening faces and voices—consistent with preclinical research in adults (Sladky et al., 2018)—variation in the degree of engagement was unrelated to the severity of social anxiety symptoms (Figure 4).

During the anticipation phase of the MSTC paradigm, the EAc (Ce and BST) was much more strongly recruited, on average, by uncertain social threat compared to either certain threat or uncertain safety. Within the BST (but not the Ce), these normative mean differences are further moderated by individual differences in the severity of social anxiety symptoms. Adolescents with more severe symptoms show blunted BST activation during the uncertain anticipation of hostile social cues, and amplified activation during the uncertain anticipation of benign ones. Might this pattern of results simply reflect heightened BST reactivity to benign social stimuli (Figure 1)? After all, socially anxious adolescents and adults often experience heightened levels of dread and discomfort during the anticipation or experience of positive social interactions (e.g., receiving praise; Fredrick & Luebbe, 2020; Weeks et al., 2019), perceive positive and neutral facial expressions as less approachable and more arousing (Kivity & Huppert, 2016), and in some cases have been shown to exhibit exaggerated amygdala activation to positive and neutral faces (Birbaumer et al., 1998; Cooney et al., 2006; Crane et al., 2021; Straube et al., 2005). The answer appears to be "no," insofar as our results demonstrate that social anxiety was unrelated to EAc activation during the acute presentation of social cues. When viewing faces and voices, the EAc is more responsive to threatening than benign cues, independent of social anxiety. This observation is consistent with work in adults with SAD (Ziv et al., 2013) and contraindicates a straightforward "hyperreactivity to benign social cues" explanation. Variation in the severity of social anxiety was also unrelated to EAc activation during the certain anticipation of threat, contraindicating the possibility that socially anxious adolescents are simply more pessimistic in their expectations or nonspecifically hyperreactive to anticipated social encounters. What mechanism, then, might explain this pattern of results? Grupe and Nitschke's conceptual framework argues that (a) uncertainty amplifies the salience of anticipated encounters with threat and (b) anxious individuals have difficulty discriminating threat from safety (Grupe & Nitschke, 2013). Such biases tend to manifest most clearly in "weak" situations, where there is more opportunity for individual differences in anxiety to guide thoughts, feelings, and behavior. This framework suggests that among adolescents with more severe social anxiety symptoms, the amplifying consequences of temporal uncertainty on BST activation are especially potent when anticipating weakly or ambiguously threatening social cues (unfamiliar adults emitting neutral or mildly positive expressions); comparatively weaker when anticipating more intense and normatively threatening social cues (unfamiliar adults emitting overtly hostile expressions); and absent during the certain anticipation or acute presentation of social cues. This perspective accounts for the overall pattern of mean differences across both phases of the MSTC paradigm and explains the opposing consequences of individual differences in social anxiety on BST anticipatory activity. More broadly, these observations reinforce the hypothesis that alterations in BST function underlie socially anxious adolescents' maladaptive responses to benign-but-uncertain everyday social encounters, such as anticipating an interaction with a sales associate or asking a routine question in class.

Clearly, a number of important challenges remain for future research. First, our study was focused on a racially diverse sample of adolescents. Moving forward, it will be useful to expand this to encompass larger and more demographically representative samples. Larger samples will also afford that statistical power necessary to tease apart whether the effects that we ascribe to social anxiety actually reflect associations with broader psychopathology dimensions, such as the fear disorders or the internalizing spectrum (Conway et al., 2019; Tiego et al., 2023; Watson et al., 2022). Second, our analyses relied on adolescent-reported social anxiety symptoms. While this approach is common in both research and clinical settings, recent work highlights the value of using more sophisticated multiinformant approaches to quantify the depth and breadth of social anxiety (D. Beidel et al., 2019; De Los Reyes et al., 2023; Makol et al., 2020). Third, our cross-sectional design does not license mechanistic claims. Prospective–longitudinal and intervention research will be necessary to determine whether diminished discrimination of uncertain social threat and safety in the BST forecasts the emergence of clinically significant distress and impairment, and whether this bias is normalized by clinically effective treatments. Preliminary work in rodents is encouraging (Bruzsik et al., 2021; De Bundel et al., 2016; Duvarci et al., 2009), demonstrating that the BST plays a critical role in discriminating Pavlovian threat from safety. For example, blockade of BST dopamine D2 receptor signaling has been shown to potentiate defensive responses to safety cues (CS−) and blunt defensive responses to threat cues (CS+); in contrast, stimulation of this pathway enhances the discrimination of threat from safety (De Bundel et al., 2016). Moving forward, it will be helpful to determine whether these perturbations produce parallel changes in defensive responding to uncertain social threat (e.g., novel conspecific) and safety (e.g., novel testing chamber). Fourth, although our results highlight the importance of the BST, social anxiety is a complex phenotype that likely reflects multiple distributed networks. It will be important to understand how interactions between the BST and other brain regions support variation in specific facets of pediatric social anxiety.

In conclusion, the present results demonstrate that adolescents with more severe social anxiety symptoms show reduced discrimination of uncertain social threat and safety in the BST. These discoveries

provide a neuroscientifically grounded framework for conceptualizing adolescent social anxiety and set the stage for the kinds of targeted follow-up research that will be necessary to clarify causation and, ultimately, to develop more effective or tolerable biological interventions for youth living with social anxiety. A diverse sample enriched for clinically significant levels of social anxiety, a well-controlled task, and a statistically unbiased (anatomical ROI) analytic approach enhance confidence in the robustness and translational relevance of these results.

References

Angst, J., Paksarian, D., Cui, L., Merikangas, K. R., Hengartner, M. P., Ajdacic-Gross, V., & Rössler, W. (2016). The epidemiology of common mental disorders from age 20 to 50: Results from the prospective Zurich cohort Study. *Epidemiology and Psychiatric Sciences*, *25*(1), 24–32. https://doi.org/10.1017/S204579601500027X

APA. (2022). *Diagnostic and statistical manual of mental disorders, text revision (DSM-5-TR)* (5th ed.). American Psychiatric Association.

Avants, B. B., Tustison, N. J., Song, G., Cook, P. A., Klein, A., & Gee, J. C. (2011). A reproducible evaluation of ANTs similarity metric performance in brain image registration. *Neuroimage*, *54*(3), 2033–2044. https://doi.org/10.1016/j.neuroimage.2010.09.025

Batelaan, N. M., Bosman, R. C., Muntingh, A., Scholten, W. D., Huijbregts, K. M., & van Balkom, A. (2017). Risk of relapse after antidepressant discontinuation in anxiety disorders, obsessive-compulsive disorder, and post-traumatic stress disorder: Systematic review and meta-analysis of relapse prevention trials. *BMJ*, *358*, Article j3927. https://doi.org/10.1136/bmj.j3927

Bechara, A., Tranel, D., Damasio, H., Adolphs, R., Rockland, C., & Damasio, A. R. (1995). Double dissociation of conditioning and declarative knowledge relative to the amygdala and hippocampus in humans. *Science*, *269*(5227), 1115–1118. https://doi.org/10.1126/science.7652558

Beesdo-Baum, K., & Knappe, S. (2012). Developmental epidemiology of anxiety disorders. *Child and Adolescent Psychiatric Clinics of North America*, *21*(3), 457–478. https://doi.org/10.1016/j.chc.2012.05.001

Beidel, D., Le, T.-A. P., & Willis, E. (2019). Social anxiety disorder: An update on diagnostics, epidemiology, etiology, assessment, treatment, unanswered questions, and future directions. In S. N. Compton, M. A. Villabø, & H. Kristensen (Eds.), *Pediatric anxiety disorders* (pp. 201–223). Academic Press. https://doi.org/10.1016/B978-0-12-813004-9.00010-4

Beidel, D. C., Turner, S. M., Hamlin, K., & Morris, T. L. (2000). The Social Phobia and Anxiety Inventory for Children (SPAI-C): External and discriminative validity. *Behavior Therapy*, *31*(1), 75–87. https://doi.org/10.1016/S0005-7894(00)80005-2

Beidel, D. C., Turner, S. M., & Morris, T. L. (1995). A new inventory to assess childhood social anxiety and phobia: The Social Phobia and Anxiety Inventory for Children. *Psychological Assessment*, *7*(1), 73–79. https://doi.org/10.1037/1040-3590.7.1.73

BIAC. (2022). *IXI Dataset*. Imperial College London. https://brain-development.org/ixi-dataset/

Birbaumer, N., Grodd, W., Diedrich, O., Klose, U., Erb, M., Lotze, M., Schneider, F., Weiss, U., & Flor, H. (1998). fMRI reveals amygdala activation to human faces in social phobics. *Neuroreport*, *9*(6), 1223–1226. https://doi.org/10.1097/00001756-199804200-00048

Boehme, S., Ritter, V., Tefikow, S., Stangier, U., Strauss, B., Miltner, W. H., & Straube, T. (2014). Brain activation during anticipatory anxiety in social anxiety disorder. *Social Cognitive and Affective Neuroscience*, *9*(9), 1413–1418. https://doi.org/10.1093/scan/nst129

Brühl, A. B., Delsignore, A., Komossa, K., & Weidt, S. (2014). Neuroimaging in social anxiety disorder—A meta-analytic review resulting in a new neurofunctional model. *Neuroscience & Biobehavioral Reviews*, *47*, 260–280. https://doi.org/10.1016/j.neubiorev.2014.08.003

Bruzsik, B., Biro, L., Zelena, D., Sipos, E., Szebik, H., Sarosdi, K. R., Horvath, O., Farkas, I., Csillag, V., Finszter, C. K., Mikics, E., & Toth, M. (2021). Somatostatin neurons of the bed nucleus of stria terminalis enhance associative fear memory consolidation in mice. *The Journal of Neuroscience*, *41*(9), 1982–1995. https://doi.org/10.1523/JNEUROSCI.1944-20.2020

Bunnell, B. E., Beidel, D. C., Liu, L., Joseph, D. L., & Higa-McMillan, C. (2015). The SPAIC-11 and SPAICP-11: Two brief child- and parent-rated measures of social anxiety. *Journal of Anxiety Disorders*, *36*, 103–109. https://doi.org/10.1016/j.janxdis.2015.10.002

Cain, C. K. (2023). Beyond fear, extinction, and freezing: Strategies for improving the translational value of animal conditioning research. *Current Topics in Behavioral Neurosciences*, *64*, 19–57. https://doi.org/10.1007/7854_2023_434

Chavanne, A. V., & Robinson, O. J. (2021). The overlapping neurobiology of adaptive and pathological anxiety: A meta-analysis of functional neural activation. *American Journal of Psychiatry*, *178*(2), 156–164. https://doi.org/10.1176/appi.ajp.2020.19111153

Chen, W. H., Lien, C. C., & Chen, C. C. (2022). Neuronal basis for pain-like and anxiety-like behaviors in the central nucleus of the amygdala. *Pain*, *163*(3), e463–e475. https://doi.org/10.1097/j.pain.0000000000002389

Clauss, J. A., & Blackford, J. U. (2012). Behavioral inhibition and risk for developing social anxiety disorder: A meta-analytic study. *Journal of the American Academy of Child & Adolescent Psychiatry*, *51*(10), 1066–1075.e1. https://doi.org/10.1016/j.jaac.2012.08.002

Conway, C. C., Forbes, M. K., Forbush, K. T., Fried, E. I., Hallquist, M. N., Kotov, R., Mullins-Sweatt, S. N., Shackman, A. J., Skodol, A. E., South, S. C., Sunderland, M., Waszczuk, M. A., Zald, D. H., Afzali, M. H., Bornovalova, M. A., Carragher, N., Docherty, A. R., Jonas, K. G., Krueger, R. F., & Eaton, N. R. (2019). A Hierarchical Taxonomy of Psychopathology can reform mental health research. *Perspectives on Psychological Science*, *14*(3), 419–436. https://doi.org/10.1177/1745691618810696

Cooney, R. E., Atlas, L. Y., Joormann, J., Eugène, F., & Gotlib, I. H. (2006). Amygdala activation in the processing of neutral faces in social anxiety disorder: Is neutral really neutral? *Psychiatry Research: Neuroimaging*, *148*(1), 55–59. https://doi.org/10.1016/j.pscychresns.2006.05.003

Cox, R. W. (1996). AFNI: Software for analysis and visualization of functional magnetic resonance neuroimages. *Computers and Biomedical Research*, *29*(3), 162–173. https://doi.org/10.1006/cbmr.1996.0014

Crane, N. A., Chang, F., Kinney, K. L., & Klumpp, H. (2021). Individual differences in striatal and amygdala response to emotional faces are related to symptom severity in social anxiety disorder. *NeuroImage: Clinical*, *30*, Article 102615. https://doi.org/10.1016/j.nicl.2021.102615

Cuijpers, P., Miguel, C., Ciharova, M., Harrer, M., Basic, D., Cristea, I. A., de Ponti, N., Driessen, E., Hamblen, J., Larsen, S. E., Matbouriahi, M., Papola, D., Pauley, D., Plessen, C. Y., Pfund, R. A., Setkowski, K., Schnurr, P. P., van Ballegooijen, W., Wang, Y., & Karyotaki, E. (2024). Absolute and relative outcomes of psychotherapies for eight mental disorders: A systematic review and meta-analysis. *World Psychiatry*, *23*(2), 267–275. https://doi.org/10.1002/wps.21203

Davies, C. D., Young, K., Torre, J. B., Burklund, L. J., Goldin, P. R., Brown, L. A., Niles, A. N., Lieberman, M. D., & Craske, M. G. (2017). Altered time course of amygdala activation during speech anticipation in social anxiety disorder. *Journal of Affective Disorders*, *209*, 23–29. https://doi.org/10.1016/j.jad.2016.11.014

Davis, M., Walker, D. L., Miles, L., & Grillon, C. (2010). Phasic vs sustained fear in rats and humans: Role of the extended amygdala in fear vs anxiety. *Neuropsychopharmacology*, *35*(1), 105–135. https://doi.org/10.1038/npp.2009.109

Davis, M., & Whalen, P. J. (2001). The amygdala: Vigilance and emotion. *Molecular Psychiatry*, *6*(1), 13–34. https://doi.org/10.1038/sj.mp.4000812

De Bundel, D., Zussy, C., Espallergues, J., Gerfen, C. R., Girault, J. A., & Valjent, E. (2016). Dopamine D2 receptors gate generalization of conditioned threat responses through mTORC1 signaling in the extended amygdala. *Molecular Psychiatry*, *21*(11), 1545–1553. https://doi.org/10.1038/mp.2015.210

De Los Reyes, A., Wang, M., Lerner, M. D., Makol, B. A., Fitzpatrick, O. M., & Weisz, J. R. (2023). The Operations Triad Model and youth mental health assessments: Catalyzing a paradigm shift in measurement validation. *Journal of Clinical Child & Adolescent Psychology*, *52*(1), 19–54. https://doi.org/10.1080/15374416.2022.2111684

Duvarci, S., Bauer, E. P., & Paré, D. (2009). The bed nucleus of the stria terminalis mediates inter-individual variations in anxiety and fear. *The Journal of Neuroscience*, *29*(33), 10357–10361. https://doi.org/10.1523/JNEUROSCI.2119-09.2009

Emery, N. J., Capitanio, J. P., Mason, W. A., Machado, C. J., Mendoza, S. P., & Amaral, D. G. (2001). The effects of bilateral lesions of the amygdala on dyadic social interactions in rhesus monkeys (*Macaca mulatta*). *Behavioral Neuroscience*, *115*(3), 515–544. https://doi.org/10.1037/0735-7044.115.3.515

Ernst, J., Ollmann, T. M., König, E., Pieper, L., Voss, C., Hoyer, J., Rückert, F., Knappe, S., & Beesdo-Baum, K. (2023). Social anxiety in adolescents and young adults from the general population: An epidemiological characterization of fear and avoidance in different social situations. *Current Psychology*, *42*(32), 28130–28145. https://doi.org/10.1007/s12144-022-03755-y

Eskildsen, S. F., Coupé, P., Fonov, V., Manjón, J. V., Leung, K. K., Guizard, N., Wassef, S. N., Østergaard, L. R., Collins, D. L., & the Alzheimer's Disease Neuroimaging Initiative. (2012). BEaST: Brain extraction based on nonlocal segmentation technique. *Neuroimage*, *59*(3), 2362–2373. https://doi.org/10.1016/j.neuroimage.2011.09.012

Evans, R., Clark, D. M., & Leigh, E. (2021). Are young people with primary social anxiety disorder less likely to recover following generic CBT compared to young people with other primary anxiety disorders? A systematic review and meta-analysis. *Behavioural and Cognitive Psychotherapy*, *49*(3), 352–369. https://doi.org/10.1017/S135246582000079X

Fehm, L., Beesdo, K., Jacobi, F., & Fiedler, A. (2008). Social anxiety disorder above and below the diagnostic threshold: Prevalence, comorbidity and impairment in the general population. *Social Psychiatry and Psychiatric Epidemiology*, *43*(4), 257–265. https://doi.org/10.1007/s00127-007-0299-4

Feinstein, J. S., Adolphs, R., Damasio, A., & Tranel, D. (2011). The human amygdala and the induction and experience of fear. *Current Biology*, *21*(1), 34–38. https://doi.org/10.1016/j.cub.2010.11.042

Feinstein, J. S., Adolphs, R., & Tranel, D. (2016). A tale of survival from the world of patient S. M. In D. G. Amaral & R. Adolphs (Eds.), *Living without an amygdala* (pp. 1–38). The Guilford Press.

Figel, B., Brinkmann, L., Buff, C., Heitmann, C. Y., Hofmann, D., Bruchmann, M., Becker, M. P. I., Herrmann, M. J., & Straube, T. (2019). Phasic amygdala and BNST activation during the anticipation of temporally unpredictable social observation in social anxiety disorder patients. *NeuroImage: Clinical*, *22*, Article 101735. https://doi.org/10.1016/j.nicl.2019.101735

Fox, A. S., & Kalin, N. H. (2014). A translational neuroscience approach to understanding the development of social anxiety disorder and its pathophysiology. *American Journal of Psychiatry*, *171*(11), 1162–1173. https://doi.org/10.1176/appi.ajp.2014.14040449

Fox, A. S., Oler, J. A., Shackman, A. J., Shelton, S. E., Raveendran, M., McKay, D. R., Converse, A. K., Alexander, A., Davidson, R. J., Blangero, J., Rogers, J., & Kalin, N. H. (2015). Intergenerational neural mediators of early-life anxious temperament. *Proceedings of the National Academy of Sciences*, *112*(29), 9118–9122. https://doi.org/10.1073/pnas.1508593112

Fox, A. S., Oler, J. A., Tromp, D. P., Fudge, J. L., & Kalin, N. H. (2015). Extending the amygdala in theories of threat processing. *Trends in Neurosciences*, *38*(5), 319–329. https://doi.org/10.1016/j.tins.2015.03.002

Fox, A. S., & Shackman, A. J. (2019). The central extended amygdala in fear and anxiety: Closing the gap between mechanistic and neuroimaging research. *Neuroscience Letters*, *693*, 58–67. https://doi.org/10.1016/j.neulet.2017.11.056

Fredrick, J. W., & Luebbe, A. M. (2020). Fear of positive evaluation and social anxiety: A systematic review of trait-based findings. *Journal of Affective Disorders*, *265*, 157–168. https://doi.org/10.1016/j.jad.2020.01.042

Garbin, C. P. (2024). *FZT*. Department of Psychology. https://psych.unl.edu/psycrs/statpage/comp.html

Gentili, C., Cristea, I. A., Angstadt, M., Klumpp, H., Tozzi, L., Phan, K. L., & Pietrini, P. (2016). Beyond emotions: A meta-analysis of neural response within face processing system in social anxiety. *Experimental Biology and Medicine*, *241*(3), 225–237. https://doi.org/10.1177/1535370215603514

Grabner, G., Janke, A. L., Budge, M. M., Smith, D., Pruessner, J., & Collins, D. L. (2006). Symmetric atlasing and model based segmentation: An application to the hippocampus in older adults. *Medical Image Computing and Computer-Assisted Intervention*, *9*(Pt 2), 58–66. https://doi.org/10.1007/11866763_8.

Gregory, A. M., Caspi, A., Moffitt, T. E., Koenen, K., Eley, T. C., & Poulton, R. (2007). Juvenile mental health histories of adults with anxiety disorders. *American Journal of Psychiatry*, *164*(2), 301–308. https://doi.org/10.1176/ajp.2007.164.2.301

Grogans, S. E., Hur, J., Barstead, M. G., Anderson, A. S., Islam, S., Kim, H. C., Kuhn, M., Tillman, R. M., Fox, A. S., Smith, J. F., DeYoung, K. A., & Shackman, A. J. (2024). Neuroticism/negative emotionality is associated with increased reactivity to uncertain threat in the bed nucleus of the stria terminalis, not the amygdala. *Journal of Neuroscience*, *44*(32), Article e1868232024. https://doi.org/10.1101/2023.02.09.527767

Grupe, D. W., & Nitschke, J. B. (2013). Uncertainty and anticipation in anxiety: An integrated neurobiological and psychological perspective. *Nature Reviews Neuroscience*, *14*(7), 488–501. https://doi.org/10.1038/nrn3524

Henson, R. (2007). Efficient experimental design for fMRI. In K. Friston, J. Ashburner, S. Kiebel, T. Nichols, & W. Penny (Eds.), *Statistical parametric mapping: The analysis of functional brain images* (pp. 193–210). Academic Press.

Hotelling, H. (1940). The selection of variates for use in prediction with some comments on the general problem of nuisance parameters. *The Annals of Mathematical Statistics*, *11*(3), 271–283. https://doi.org/10.1214/aoms/1177731867

Hur, J., Kaplan, C. M., Smith, J. F., Bradford, D. E., Fox, A. S., Curtin, J. J., & Shackman, A. J. (2018). Acute alcohol administration dampens central extended amygdala reactivity. *Scientific Reports*, *8*(1), Article 16702. https://doi.org/10.1038/s41598-018-34987-3

Hur, J., Kuhn, M., Grogans, S. E., Anderson, A. S., Islam, S., Kim, H. C., Tillman, R. M., Fox, A. S., Smith, J. F., DeYoung, K. A., & Shackman, A. J. (2022). Anxiety-related frontocortical activity is associated with dampened stressor reactivity in the real world. *Psychological Science*, *33*(6), 906–924. https://doi.org/10.1177/09567976211056635

Hur, J., Smith, J. F., DeYoung, K. A., Anderson, A. S., Kuang, J., Kim, H. C., Tillman, R. M., Kuhn, M., Fox, A. S., & Shackman, A. J. (2020). Anxiety and the neurobiology of temporally uncertain threat anticipation. *The Journal of Neuroscience*, *40*(41), 7949–7964. https://doi.org/10.1523/JNEUROSCI.0704-20.2020

Hur, J., Stockbridge, M. D., Fox, A. S., & Shackman, A. J. (2019). Dispositional negativity, cognition, and anxiety disorders: An integrative translational neuroscience framework. *Progress in Brain Research*, *247*, 375–436. https://doi.org/10.1016/bs.pbr.2019.03.012

Hyett, M. P., & McEvoy, P. M. (2018). Social anxiety disorder: Looking back and moving forward. *Psychological Medicine*, *48*(12), 1937–1944. https://doi.org/10.1017/S0033291717003816

Inman, C. S., Bijanki, K. R., Bass, D. I., Gross, R. E., Hamann, S., & Willie, J. T. (2020). Human amygdala stimulation effects on emotion physiology and emotional experience. *Neuropsychologia*, *145*, Article 106722. https://doi.org/10.1016/j.neuropsychologia.2018.03.019

James, A. C., Reardon, T., Soler, A., James, G., & Creswell, C. (2020). Cognitive behavioural therapy for anxiety disorders in children and adolescents. *Cochrane Database of Systematic Reviews*, *11*(11), Article CD013162. https://doi.org/10.1002/14651858.CD013162.pub2

Jarcho, J. M., Leibenluft, E., Walker, O. L., Fox, N. A., Pine, D. S., & Nelson, E. E. (2013). Neuroimaging studies of pediatric social anxiety: Paradigms, pitfalls and a new direction for investigating the neural mechanisms. *Biology of Mood & Anxiety Disorders*, *3*(1), Article 14. https://doi.org/10.1186/2045-5380-3-14

Jenkinson, M., Beckmann, C. F., Behrens, T. E., Woolrich, M. W., & Smith, S. M. (2012). FSL. *Neuroimage*, *62*(2), 782–790. https://doi.org/10.1016/j.neuroimage.2011.09.015

Jystad, I., Bjerkeset, O., Haugan, T., Sund, E. R., & Vaag, J. (2021). Sociodemographic correlates and mental health comorbidities in adolescents with social anxiety: The Young-HUNT3 Study, Norway. *Frontiers in Psychology*, *12*, Article 663161. https://doi.org/10.3389/fpsyg.2021.663161

Kalin, N. H., Fox, A. S., Kovner, R., Riedel, M. K., Fekete, E. M., Roseboom, P. H., Tromp, P. M., Grabow, B. P., Olsen, M. E., Brodsky, E. K., McFarlin, D. R., Alexander, A. L., Emborg, M. E., Block, W. F., Fudge, J. L., & Oler, J. A. (2016). Overexpressing corticotropin-releasing hormone in the primate amygdala increases anxious temperament and alters its neural circuit. *Biological Psychiatry*, *80*(5), 345–355. https://doi.org/10.1016/j.biopsych.2016.01.010

Kalin, N. H., Shelton, S. E., & Davidson, R. J. (2004). The role of the central nucleus of the amygdala in mediating fear and anxiety in the primate. *The Journal of Neuroscience*, *24*(24), 5506–5515. https://doi.org/10.1523/JNEUROSCI.0292-04.2004

Katzelnick, D. J., Kobak, K. A., DeLeire, T., Henk, H. J., Greist, J. H., Davidson, J. R., Schneier, F. R., Stein, M. B., & Helstad, C. P. (2001). Impact of generalized social anxiety disorder in managed care. *American Journal of Psychiatry*, *158*(12), 1999–2007. https://doi.org/10.1176/appi.ajp.158.12.1999

Kessler, R. C. (2003). The impairments caused by social phobia in the general population: Implications for intervention. *Acta Psychiatrica Scandinavica*, *108*(s417), 19–27. https://doi.org/10.1034/j.1600-0447.108.s417.2.x

Kessler, R. C., Petukhova, M., Sampson, N. A., Zaslavsky, A. M., & Wittchen, H. U. (2012). Twelve-month and lifetime prevalence and lifetime morbid risk of anxiety and mood disorders in the United States. *International Journal of Methods in Psychiatric Research*, *21*(3), 169–184. https://doi.org/10.1002/mpr.1359

Kim, H. C., Kaplan, C. M., Islam, S., Anderson, A. S., Piper, M. E., Bradford, D. E., Curtin, J. J., DeYoung, K. A., Smith, J. F., Fox, A. S., & Shackman, A. J. (2023). Acute nicotine abstinence amplifies subjective withdrawal symptoms and threat-evoked fear and anxiety, but not extended amygdala reactivity. *PLoS ONE*, *18*(7), Article e0288544. https://doi.org/10.1371/journal.pone.0288544

Kivity, Y., & Huppert, J. D. (2016). Emotional reactions to facial expressions in social anxiety: A meta-analysis of self-reports. *Emotion Review*, *8*(4), 367–375. https://doi.org/10.1177/1754073915594436

Klumpp, H., & Fitzgerald, J. M. (2018). Neuroimaging predictors and mechanisms of treatment response in Social Anxiety Disorder: An overview of the amygdala. *Current Psychiatry Reports*, *20*(10), Article 89. https://doi.org/10.1007/s11920-018-0948-1

Korn, C. W., Vunder, J., Miró, J., Fuentemilla, L., Hurlemann, R., & Bach, D. R. (2017). Amygdala lesions reduce anxiety-like behavior in a human benzodiazepine-sensitive approach-avoidance conflict test. *Biological Psychiatry*, *82*(7), 522–531. https://doi.org/10.1016/j.biopsych.2017.01.018

Koyuncu, A., İnce, E., Ertekin, E., & Tükel, R. (2019). Comorbidity in social anxiety disorder: Diagnostic and therapeutic challenges. *Drugs in Context*, *8*, Article 212573. https://doi.org/10.7573/dic.212573

Krüger, O., Shiozawa, T., Kreifelts, B., Scheffler, K., & Ethofer, T. (2015). Three distinct fiber pathways of the bed nucleus of the stria terminalis to the amygdala and prefrontal cortex. *Cortex*, *66*, 60–68. https://doi.org/10.1016/j.cortex.2015.02.007

Lahey, B. B., Tiemeier, H., & Krueger, R. F. (2022). Seven reasons why binary diagnostic categories should be replaced with empirically sounder and less stigmatizing dimensions. *JCPP Advances*, *2*(4), Article e12108. https://doi.org/10.1002/jcv2.12108

Lange, M. D., Daldrup, T., Remmers, F., Szkudlarek, H. J., Lesting, J., Guggenhuber, S., Ruehle, S., Jüngling, K., Seidenbecher, T., Lutz, B., & Pape, H. C. (2017). Cannabinoid CB1 receptors in distinct circuits of the extended amygdala determine fear responsiveness to unpredictable threat. *Molecular Psychiatry*, *22*(10), 1422–1430. https://doi.org/10.1038/mp.2016.156

Lee, Y., Fitz, S., Johnson, P. L., & Shekhar, A. (2008). Repeated stimulation of CRF receptors in the BNST of rats selectively induces social but not panic-like anxiety. *Neuropsychopharmacology*, *33*(11), 2586–2594. https://doi.org/10.1038/sj.npp.1301674

Lipsitz, J. D., & Schneier, F. R. (2000). Social phobia. Epidemiology and cost of illness. *PharmacoEconomics*, *18*(1), 23–32. https://doi.org/10.2165/00019053-200018010-00003

Lorberbaum, J. P., Kose, S., Johnson, M. R., Arana, G. W., Sullivan, L. K., Hamner, M. B., Ballenger, J. C., Lydiard, R. B., Brodrick, P. S., Bohning, D. E., & George, M. S. (2004). Neural correlates of speech anticipatory anxiety in generalized social phobia. *Neuroreport*, *15*(18), 2701–2705. https://doi.org/10.1097/01.wnr.0000148724.96232.e7

Lungwitz, E. A., Molosh, A., Johnson, P. L., Harvey, B. P., Dirks, R. C., Dietrich, A., Minick, P., Shekhar, A., & Truitt, W. A. (2012). Orexin-A induces anxiety-like behavior through interactions with glutamatergic receptors in the bed nucleus of the stria terminalis of rats. *Physiology & Behavior*, *107*(5), 726–732. https://doi.org/10.1016/j.physbeh.2012.05.019

Ma, D. S., Correll, J., & Wittenbrink, B. (2015). The Chicago face database: A free stimulus set of faces and norming data. *Behavior Research Methods*, *47*(4), 1122–1135. https://doi.org/10.3758/s13428-014-0532-5

Makol, B. A., Youngstrom, E. A., Racz, S. J., Qasmieh, N., Glenn, L. E., & De Los Reyes, A. (2020). Integrating multiple informants' reports: How conceptual and measurement models may address long-standing problems in clinical decision-making. *Clinical Psychological Science*, *8*(6), 953–970. https://doi.org/10.1177/2167702620924439

Mathew, A. R., Pettit, J. W., Lewinsohn, P. M., Seeley, J. R., & Roberts, R. E. (2011). Co-morbidity between major depressive disorder and anxiety disorders: Shared etiology or direct causation? *Psychological Medicine*, *41*(10), 2023–2034. https://doi.org/10.1017/S0033291711000407

McCormick, M., Liu, X., Jomier, J., Marion, C., & Ibanez, L. (2014). ITK: Enabling reproducible research and open science. *Frontiers in Neuroinformatics*, *8*, Article 13. https://doi.org/10.3389/fninf.2014.00013

Merikangas, K. R., Avenevoli, S., Acharyya, S., Zhang, H., & Angst, J. (2002). The spectrum of social phobia in the Zurich cohort study of young adults. *Biological Psychiatry*, *51*(1), 81–91. https://doi.org/10.1016/S0006-3223(01)01309-9

Meyer, C., Padmala, S., & Pessoa, L. (2019). Dynamic threat processing. *Journal of Cognitive Neuroscience*, *31*(4), 522–542. https://doi.org/10.1162/jocn_a_01363

Michalska, K. J., Benson, B., Ivie, E. J., Sachs, J. F., Haller, S. P., Abend, R., McFarlin, D. R., Blackford, J. U., & Pine, D. S. (2023). Neural responding during uncertain threat anticipation in pediatric anxiety. *International Journal of Psychophysiology*, *183*, 159–170. https://doi.org/10.1016/j.ijpsycho.2022.07.006

Moscarello, J. M., & Penzo, M. A. (2022). The central nucleus of the amygdala and the construction of defensive modes across the threat-imminence

continuum. *Nature Neuroscience*, *25*(8), 999–1008. https://doi.org/10.1038/s41593-022-01130-5

Mumford, J. A., Poline, J. B., & Poldrack, R. A. (2015). Orthogonalization of regressors in FMRI models. *PLoS ONE*, *10*(4), Article e0126255. https://doi.org/10.1371/journal.pone.0126255

Murty, D. V. P. S., Song, S., Surampudi, S. G., & Pessoa, L. (2023). Threat and reward imminence processing in the human brain. *The Journal of Neuroscience*, *43*(16), 2973–2987. https://doi.org/10.1523/JNEUROSCI.1778-22.2023

NIMH. (2011). *Negative valence systems: Workshop proceedings*. https://www.nimh.nih.gov/research/research-funded-by-nimh/rdoc/negative-valence-systems-workshop-proceedings.shtml

Oler, J. A., Fox, A. S., Shackman, A. J., & Kalin, N. H. (2016). The central nucleus of the amygdala is a critical substrate for individual differences in anxiety. In D. G. Amaral & R. Adolphs (Eds.), *Living without an amygdala* (pp. 218–251). Guilford.

Petersen, A. C., Crockett, L., Richards, M., & Boxer, A. (1988). *Pubertal Development Scale (PDS)*. APA PsycTests. https://doi.org/10.1037/t06349-000

Poldrack, R. A., Baker, C. I., Durnez, J., Gorgolewski, K. J., Matthews, P. M., Munafò, M. R., Nichols, T. E., Poline, J. B., Vul, E., & Yarkoni, T. (2017). Scanning the horizon: Towards transparent and reproducible neuroimaging research. *Nature Reviews Neuroscience*, *18*(2), 115–126. https://doi.org/10.1038/nrn.2016.167

Poline, J., Kherif, F., Pallier, C., & Penny, W. (2007). Contrasts and classical inference. In L. Friston (Ed.), *Statistical parametric mapping: The analysis of functional brain images* (pp. 126–139). Elsevier.

Pomrenze, M. B., Giovanetti, S. M., Maiya, R., Gordon, A. G., Kreeger, L. J., & Messing, R. O. (2019). Dissecting the roles of GABA and neuropeptides from rat central amygdala CRF neurons in anxiety and fear learning. *Cell Reports*, *29*(1), 13–21.e4. https://doi.org/10.1016/j.celrep.2019.08.083

Pomrenze, M. B., Tovar-Diaz, J., Blasio, A., Maiya, R., Giovanetti, S. M., Lei, K., Morikawa, H., Hopf, F. W., & Messing, R. O. (2019). A corticotropin releasing factor network in the extended amygdala for anxiety. *The Journal of Neuroscience*, *39*(6), 1030–1043. https://doi.org/10.1523/JNEUROSCI.2143-18.2018

Pruim, R. H. R., Mennes, M., van Rooij, D., Llera, A., Buitelaar, J. K., & Beckmann, C. F. (2015). ICA-AROMA: A robust ICA-based strategy for removing motion artifacts from fMRI data. *Neuroimage*, *112*, 267–277. https://doi.org/10.1016/j.neuroimage.2015.02.064

R Core Team. (2022). *R: A language and environment for statistical computing* [Computer software]. R Foundation for Statistical Computing. https://finzi.psych.upenn.edu/R/library/dplR/doc/intro-dplR.pdf

Rapee, R. M., McLellan, L. F., Carl, T., Trompeter, N., Hudson, J. L., Jones, M. P., & Wuthrich, V. M. (2023). Comparison of transdiagnostic treatment and specialized social anxiety treatment for children and adolescents with Social Anxiety Disorder: A randomized controlled trial. *Journal of the American Academy of Child & Adolescent Psychiatry*, *62*(6), 646–655. https://doi.org/10.1016/j.jaac.2022.08.003

Ren, J., Lu, C. L., Huang, J., Fan, J., Guo, F., Mo, J. W., Huang, W. Y., Kong, P. L., Li, X. W., Sun, L. R., Sun, X. D., & Cao, X. (2022). A distinct metabolically defined central nucleus circuit bidirectionally controls anxiety-related behaviors. *The Journal of Neuroscience*, *42*(11), 2356–2370. https://doi.org/10.1523/JNEUROSCI.1578-21.2022

Ressler, R. L., Goode, T. D., Evemy, C., & Maren, S. (2020). NMDA receptors in the CeA and BNST differentially regulate fear conditioning to predictable and unpredictable threats. *Neurobiology of Learning and Memory*, *174*, Article 107281. https://doi.org/10.1016/j.nlm.2020.107281

RStudio Team. (2022). *RStudio: Integrated development for R*. RStudio PBC.

Sajdyk, T., Johnson, P., Fitz, S., & Shekhar, A. (2008). Chronic inhibition of GABA synthesis in the bed nucleus of the stria terminalis elicits anxiety-like behavior. *Journal of Psychopharmacology*, *22*(6), 633–641. https://doi.org/10.1177/0269881107082902

Schneier, F. R., Blanco, C., Antia, S. X., & Liebowitz, M. R. (2002). The social anxiety spectrum. *Psychiatric Clinics of North America*, *25*(4), 757–774. https://doi.org/10.1016/S0193-953X(02)00018-7

Schneier, F. R., Johnson, J., Hornig, C. D., Liebowitz, M. R., & Weissman, M. M. (1992). Social phobia: Comorbidity and morbidity in an epidemiologic sample. *Archives of General Psychiatry*, *49*(4), 282–288. https://doi.org/10.1001/archpsyc.1992.01820040034004

Scholten, W. D., Batelaan, N. M., Penninx, B. W., van Balkom, A. J., Smit, J. H., Schoevers, R. A., & van Oppen, P. (2016). Diagnostic instability of recurrence and the impact on recurrence rates in depressive and anxiety disorders. *Journal of Affective Disorders*, *195*, 185–190. https://doi.org/10.1016/j.jad.2016.02.025

Scholten, W. D., Batelaan, N. M., van Balkom, A. J., Wjh Penninx, B., Smit, J. H., & van Oppen, P. (2013). Recurrence of anxiety disorders and its predictors. *Journal of Affective Disorders*, *147*(1–3), 180–185. https://doi.org/10.1016/j.jad.2012.10.031

Shackman, A. J., & Fox, A. S. (2016). Contributions of the central extended amygdala to fear and anxiety. *Journal of Neuroscience*, *36*(31), 8050–8063. https://doi.org/10.1523/JNEUROSCI.0982-16.2016

Shackman, A. J., & Fox, A. S. (2018). Getting serious about variation: Lessons for clinical neuroscience. *Trends in Cognitive Sciences*, *22*(5), 368–369. https://doi.org/10.1016/j.tics.2018.02.009

Shackman, A. J., & Fox, A. S. (2021). Two decades of anxiety neuroimaging research: New insights and a look to the future. *American Journal of Psychiatry*, *178*(2), 106–109. https://doi.org/10.1176/appi.ajp.2020.20121733

Shackman, A. J., Fox, A. S., Oler, J. A., Shelton, S. E., Davidson, R. J., & Kalin, N. H. (2013). Neural mechanisms underlying heterogeneity in the presentation of anxious temperament. *Proceedings of the National Academy of Sciences*, *110*(15), 6145–6150. https://doi.org/10.1073/pnas.1214364110

Shackman, A. J., Grogans, S. E., & Fox, A. S. (2024). Fear, anxiety, and the functional architecture of the human central extended amygdala. *Nature Reviews Neuroscience*, *25*(8), 587–588. https://doi.org/10.1038/s41583-024-00832-y

Shackman, A. J., Stockbridge, M. D., Tillman, R. M., Kaplan, C. M., Tromp, D. P. M., Fox, A. S., & Gamer, M. (2016). The neurobiology of anxiety and attentional biases to threat: Implications for understanding anxiety disorders in adults and youth. *Journal of Experimental Psychopathology*, *7*(3), 311–342. https://doi.org/10.5127/jep.054015

Sheehan, D. V., Sheehan, K. H., Shytle, R. D., Janavs, J., Bannon, Y., Rogers, J. E., Milo, K. M., Stock, S. L., & Wilkinson, B. (2010). Reliability and validity of the Mini International Neuropsychiatric Interview for Children and Adolescents (MINI-KID). *The Journal of Clinical Psychiatry*, *71*(3), 313–326. https://doi.org/10.4088/JCP.09m05305whi

Singewald, N., Sartori, S. B., Reif, A., & Holmes, A. (2023). Alleviating anxiety and taming trauma: Novel pharmacotherapeutics for anxiety disorders and posttraumatic stress disorder. *Neuropharmacology*, *226*, Article 109418. https://doi.org/10.1016/j.neuropharm.2023.109418

Sladky, R., Geissberger, N., Pfabigan, D. M., Kraus, C., Tik, M., Woletz, M., Paul, K., Vanicek, T., Auer, B., Kranz, G. S., Lamm, C., Lanzenberger, R., & Windischberger, C. (2018). Unsmoothed functional MRI of the human amygdala and bed nucleus of the stria terminalis during processing of emotional faces. *Neuroimage*, *168*, 383–391. https://doi.org/10.1016/j.neuroimage.2016.12.024

Spinhoven, P., Batelaan, N., Rhebergen, D., van Balkom, A., Schoevers, R., & Penninx, B. W. (2016). Prediction of 6-yr symptom course trajectories of anxiety disorders by diagnostic, clinical and psychological variables. *Journal of Anxiety Disorders*, *44*, 92–101. https://doi.org/10.1016/j.janxdis.2016.10.011

Stein, D. J., Lim, C. C. W., Roest, A. M., de Jonge, P., Aguilar-Gaxiola, S., Al-Hamzawi, A., Alonso, J., Benjet, C., Bromet, E. J., Bruffaerts, R., de Girolamo, G., Florescu, S., Gureje, O., Haro, J. M., Harris, M. G., He,

Y., Hinkov, H., Horiguchi, I., Hu, C., … & the WHO World Mental Health Survey Collaborators. (2017). The cross-national epidemiology of social anxiety disorder: Data from the World Mental Health Survey Initiative. *BMC Medicine*, *15*(1), Article 143. https://doi.org/10.1186/s12916-017-0889-2

Straube, T., Mentzel, H. J., & Miltner, W. H. (2005). Common and distinct brain activation to threat and safety signals in social phobia. *Neuropsychobiology*, *52*(3), 163–168. https://doi.org/10.1159/000087987

Strawn, J. R., Lu, L., Peris, T. S., Levine, A., & Walkup, J. T. (2021). Pediatric anxiety disorders–what have we learnt in the last 10 years? *Journal of Child Psychology and Psychiatry*, *62*(2), 114–139. https://doi.org/10.1111/jcpp.13262

Tan, E., Zeytinoglu, S., Morales, S., Buzzell, G. A., Almas, A. N., Degnan, K. A., Chronis-Tuscano, A., Henderson, H., Pine, D. S., & Fox, N. A. (2024). Social versus non-social behavioral inhibition: Differential prediction from early childhood of long-term psychosocial outcomes. *Developmental Science*, *27*(1), Article e13427. https://doi.org/10.1111/desc.13427

Theiss, J. D., Ridgewell, C., McHugo, M., Heckers, S., & Blackford, J. U. (2017). Manual segmentation of the human bed nucleus of the stria terminalis using 3T MRI. *Neuroimage*, *146*, 288–292. https://doi.org/10.1016/j.neuroimage.2016.11.047

Tiego, J., Martin, E., DeYoung, C. G., Hagan, K., Cooper, S. E., Pasion, R., Satchell, L., Shackman, A. J., Bellgrove, M. A., Fornito, A., & The HiTOP Neurobiological Foundations Work Group. (2023). Precision behavioral phenotyping as a strategy for uncovering the biological correlates of psychopathology. *Nature Mental Health*, *1*(5), 304–315. https://doi.org/10.1038/s44220-023-00057-5

Tillfors, M., Furmark, T., Marteinsdottir, I., & Fredrikson, M. (2002). Cerebral blood flow during anticipation of public speaking in social phobia: A PET study. *Biological Psychiatry*, *52*(11), 1113–1119. https://doi.org/10.1016/S0006-3223(02)01396-3

Tillman, R. M., Stockbridge, M. D., Nacewicz, B. M., Torrisi, S., Fox, A. S., Smith, J. F., & Shackman, A. J. (2018). Intrinsic functional connectivity of the central extended amygdala. *Human Brain Mapping*, *39*(3), 1291–1312. https://doi.org/10.1002/hbm.23917

Tranel, D., Gullickson, G., Koch, M., & Adolphs, R. (2006). Altered experience of emotion following bilateral amygdala damage. *Cognitive Neuropsychiatry*, *11*(3), 219–232. https://doi.org/10.1080/13546800444000281

Tseng, Y.-T., Schaefke, B., Wei, P., & Wang, L. (2023). Defensive responses: Behaviour, the brain and the body. *Nature Reviews Neuroscience*, *24*(11), 655–671. https://doi.org/10.1038/s41583-023-00736-3

Tukey, J. W. (1977). *Exploratory data analysis*. Addison Wesley.

Tulbure, B. T., Szentagotai, A., Dobrean, A., & David, D. (2012). Evidence based clinical assessment of child and adolescent social phobia: A critical review of rating scales. *Child Psychiatry & Human Development*, *43*(5), 795–820. https://doi.org/10.1007/s10578-012-0297-y

Tustison, N. J., Avants, B. B., Cook, P. A., Zheng, Y., Egan, A., Yushkevich, P. A., & Gee, J. C. (2010). N4ITK: Improved N3 bias correction. *IEEE Transactions on Medical Imaging*, *29*(6), 1310–1320. https://doi.org/10.1109/TMI.2010.2046908

Watson, D., Levin-Aspenson, H. F., Waszczuk, M. A., Conway, C. C., Dalgleish, T., Dretsch, M. N., Eaton, N. R., Forbes, M. K., Forbush, K. T., Hobbs, K. A., Michelini, G., Nelson, B. D., Sellbom, M., Slade, T., South, S. C., Sunderland, M., Waldman, I., Witthöft, M., Wright, A. G. C., … & HiTOP Utility Workgroup. (2022). Validity and utility of Hierarchical Taxonomy of Psychopathology (HiTOP): III. Emotional dysfunction superspectrum. *World Psychiatry*, *21*(1), 26–54. https://doi.org/10.1002/wps.20943

Weeks, J. W., Howell, A. N., Srivastav, A., & Goldin, P. R. (2019). "Fear guides the eyes of the beholder": Assessing gaze avoidance in social anxiety disorder via covert eye tracking of dynamic social stimuli. *Journal of Anxiety Disorders*, *65*, 56–63. https://doi.org/10.1016/j.janxdis.2019.05.005

Wellcome Centre for Human Neuroimaging. (2022). *SPM*. University College London. Retrieved April 18 from https://fil.ion.ucl.ac.uk/spm/

Wickham, H. (2016). *Ggplot2: Elegant graphics for data analysis* (2nd ed.). Springer-Verlag.

Wong, Q. J., Gregory, B., & McLellan, L. F. (2016). A review of scales to measure social anxiety disorder in clinical and epidemiological studies. *Current Psychiatry Reports*, *18*(4), Article 38. https://doi.org/10.1007/s11920-016-0677-2

Zhu, Y., Xie, S. Z., Peng, A. B., Yu, X. D., Li, C. Y., Fu, J. Y., Shen, C. J., Cao, S. X., Zhang, Y., Chen, J., & Li, X. M. (2024). Distinct circuits from the central lateral amygdala to the ventral part of the bed nucleus of stria terminalis regulate different fear memory. *Biological Psychiatry*, *95*(8), 732–744. https://doi.org/10.1016/j.biopsych.2023.08.022

Ziv, M., Goldin, P. R., Jazaieri, H., Hahn, K. S., & Gross, J. J. (2013). Is there less to social anxiety than meets the eye? Behavioral and neural responses to three socio-emotional tasks. *Biology of Mood & Anxiety Disorders*, *3*(1), Article 5. https://doi.org/10.1186/2045-5380-3-5

Received November 13, 2023
Revision received May 29, 2024
Accepted June 24, 2024 ■

Supplementary Results

Juyoen Hur[1]*
Rachael M. Tillman[2]*
Hyung Cho Kim[3,4]
Paige Didier[3]
Allegra S. Anderson[7]
Samiha Islam[8]
Melissa D. Stockbridge[9]
Andres De Los Reyes[3]
Kathryn A. DeYoung[3,6]
Jason F. Smith[3]
Alexander J. Shackman[3,4,5]

[1]Department of Psychology, Yonsei University, Seoul 03722, Republic of Korea. [2]Department of Neuropsychology, Children's National Hospital, Washington, DC 20010 USA. [3]Department of Psychology, [4]Neuroscience and Cognitive Science Program, and [5]Maryland Neuroimaging Center, University of Maryland, College Park, MD 20742 USA. [6]TheraQuest LLC, Bethesda, MD 20817. [7]Department of Psychological Sciences, Vanderbilt University, Nashville, TN 37240 USA. [8]Department of Psychology, University of Pennsylvania, Philadelphia, PA 19104 USA. [9]Department of Neurology, School of Medicine, Johns Hopkins University, Baltimore, MD 21287 USA.

* contributed equally

Address Correspondence to:
Juyoen Hur (jhur1@yonsei.ac.kr) or Alexander J. Shackman (shackman@umd.edu)

Table S1. Descriptive statistics for clusters and local extrema showing omnibus differences in activation between the three Anticipation conditions (Uncertain Threat, Certain Threat, and Uncertain Safety) relative to implicit baseline (Certain Safety Anticipation), $p<.05$, whole-brain corrected.

Cluster	Hemisphere	Label	mm^3	*F*	*x*	*y*	*z*
1	L	Cuneal Cortex	86,824	8.96	-12	-80	30
1	L	Intracalcarine Cortex	86,824	89.58	-14	-74	8
1	L	Lateral Occipital Cortex, superior division	86,824	10.68	-12	-84	46
1	L	Lingual Gyrus	86,824	17.71	-18	-52	-10
1	L	Occipital Fusiform Gyrus	86,824	32.06	-28	-72	-12
1	L	Occipital Pole	86,824	61.57	-8	-98	-4
1	L	Temporal Occipital Fusiform Cortex	86,824	23.56	-32	-58	-14
1	R	Cuneal Cortex	86,824	26.25	4	-86	34
1	R	Intracalcarine Cortex	86,824	130.35	14	-78	12
1	R	Lingual Gyrus	86,824	17.54	18	-44	-10
1	R	Occipital Fusiform Gyrus	86,824	43.76	26	-76	-12
1	R	Occipital Pole	86,824	69.28	8	-90	-2
1	R	Supracalcarine Cortex	86,824	104.29	2	-80	8
1	R	Temporal Occipital Fusiform Cortex	86,824	14.71	28	-48	-12
2	L	Postcentral Gyrus	48,576	8.68	-14	-46	70
2	L	Precuneus Cortex	48,576	16.41	-10	-50	58
2	L	Superior Parietal Lobule	48,576	17.66	-28	-46	60
2	R	Angular Gyrus	48,576	17.94	60	-46	22
2	R	Lateral Occipital Cortex, inferior division	48,576	46.47	48	-72	0
2	R	Lateral Occipital Cortex, superior division	48,576	23.03	48	-68	20
2	R	Middle Temporal Gyrus, temporooccipital part	48,576	23.57	60	-46	2
2	R	Postcentral Gyrus	48,576	14.62	42	-36	58
2	R	Precuneus Cortex	48,576	16.16	8	-48	54
2	R	Superior Parietal Lobule	48,576	18.55	26	-50	52
2	R	Supramarginal Gyrus, posterior division	48,576	17.66	44	-38	50
2	R	Temporal Occipital Fusiform Cortex	48,576	27.99	44	-50	-16
3	R	Middle Frontal Gyrus	8,360	11.27	28	12	54
3	R	Precentral Gyrus	8,360	18.63	26	-12	66
3	R	Superior Frontal Gyrus	8,360	15.01	20	-2	58
4	L	Middle Frontal Gyrus	8,080	11.80	-38	4	46
4	L	Paracingulate Gyrus	8,080	14.49	-10	12	44
4	L	Precentral Gyrus	8,080	16.97	-32	-10	56
4	L	Superior Frontal Gyrus	8,080	15.40	-12	6	64
4	R	Midcingulate Cortex	8,080	17.13	6	8	26
4	R	Paracingulate Gyrus	8,080	9.35	6	14	40
5	R	Inferior Frontal Gyrus, pars opercularis	7,576	21.36	40	12	26

5	R	Precentral Gyrus	7,576	30.19	46	8	32
6	R	Frontal Pole/ dorsolateral Prefronal Cortex	3,216	14.79	26	42	28
6	R	Middle Frontal Gyrus	3,216	12.03	32	34	32
7	L	Inferior Temporal Gyrus, temporooccipital part	2,800	15.91	-46	-62	-12
7	L	Middle Temporal Gyrus, posterior division	2,800	10.41	-58	-44	-2
7	L	Middle Temporal Gyrus, temporooccipital part	2,800	12.94	-56	-50	2
8	L	Midcingulate Cortex	1,096	11.69	-10	24	26
9	L	Lateral Occipital Cortex, superior division	1,096	13.78	-22	-76	36

Table S2. Descriptive statistics for clusters and local extrema showing greater activation during the uncertain versus certain anticipation of threatening faces and voices (masked by the omnibus *F*-test), $p<.05$, whole-brain corrected.

Cluster	Hemisphere	Label	mm^3	*t*	*x*	*y*	*z*
1	R	Angular Gyrus	38,152	5.57	62	-46	18
1	R	Lateral Occipital Cortex, inferior division	38,152	8.48	52	-72	-2
1	R	Lateral Occipital Cortex, superior division	38,152	4.95	22	-68	42
1	R	Middle Temporal Gyrus, temporooccipital part	38,152	6.95	60	-46	2
1	R	Postcentral Gyrus	38,152	4.87	42	-36	58
1	R	Superior Parietal Lobule	38,152	5.17	24	-50	54
1	R	Supramarginal Gyrus, posterior division	38,152	5.78	42	-40	48
1	R	Temporal Occipital Fusiform Cortex	38,152	6.74	44	-50	-18
2	L	Postcentral Gyrus	8,064	4.22	-14	-46	70
2	L	Precuneus Cortex	8,064	5.65	-10	-50	56
2	L	Superior Parietal Lobule	8,064	6.00	-28	-46	60
2	R	Lateral Occipital Cortex, superior division	8,064	4.47	14	-62	54
2	R	Precuneus Cortex	8,064	5.72	10	-46	52
3	R	Middle Frontal Gyrus	7,624	4.78	28	12	54
3	R	Precentral Gyrus	7,624	5.11	38	-6	50
3	R	Superior Frontal Gyrus	7,624	5.14	22	4	52
4	R	Inferior Frontal Gyrus, pars opercularis	7,576	6.33	40	12	26
4	R	Precentral Gyrus	7,576	7.63	44	6	32
5	L	Middle Frontal Gyrus	7,432	4.76	-40	4	46
5	L	Paracingulate Gyrus	7,432	5.46	-10	12	44
5	L	Precentral Gyrus	7,432	5.38	-32	-8	56
5	L	Superior Frontal Gyrus	7,432	4.81	-26	0	62
5	R	Midcingulate Cortex	7,432	4.89	8	24	28
5	R	Paracingulate Gyrus	7,432	4.08	2	12	42
6	R	Frontal Pole	3,184	5.29	26	42	28
7	L	Inferior Temporal Gyrus, temporooccipital part	2,648	5.49	-46	-62	-12
7	L	Middle Temporal Gyrus, posterior division	2,648	4.32	-58	-44	-2
7	L	Middle Temporal Gyrus, temporooccipital part	2,648	4.87	-56	-50	4
8	L	Midcingulate Cortex	1,080	4.79	-10	24	26
9	L	Lateral Occipital Cortex, superior division	1,072	5.29	-24	-76	36
10	R	Midcingulate Cortex	384	5.29	4	12	24
11	L	Cuneal Cortex	40	3.68	-12	-82	30

Table S3. Descriptive statistics for clusters and local extrema showing greater activation during the certain versus uncertain anticipation of threatening faces and voices (masked by the omnibus *F*-test), $p<.05$, whole-brain corrected.

Cluster	**Hemisphere**	**Label**	**mm³**	***t***	***x***	***y***	***z***
1	L	Intracalcarine Cortex	82,288	11.82	-14	-74	6
1	L	Lateral Occipital Cortex, inferior division	82,288	4.06	-38	-86	-16
1	L	Lingual Gyrus	82,288	5.57	-18	-52	-10
1	L	Occipital Fusiform Gyrus	82,288	7.64	-28	-76	-12
1	L	Occipital Pole	82,288	11.13	-8	-98	-4
1	L	Temporal Occipital Fusiform Cortex	82,288	6.57	-32	-58	-14
1	R	Cuneal Cortex	82,288	7.03	2	-86	36
1	R	Intracalcarine Cortex	82,288	11.50	12	-88	2
1	R	Occipital Fusiform Gyrus	82,288	9.19	26	-76	-12
1	R	Occipital Pole	82,288	11.94	6	-90	-2
1	R	Supracalcarine Cortex	82,288	12.56	2	-80	8
2	R	Lingual Gyrus	504	4.98	18	-44	-10
2	R	Temporal Occipital Fusiform Cortex	504	3.33	26	-48	-14

Table S4. Descriptive statistics for clusters and local extrema showing greater activation during the uncertain anticipation of threatening versus benign faces and voices (masked by the omnibus *F*-test), $p<.05$, whole-brain corrected.

Cluster	**Hemisphere**	**Label**	**mm³**	***t***	***x***	***y***	***z***
1	L	Precuneus Cortex	3,640	5.16	-6	-50	54
1	R	Cingulate Gyrus, posterior division	3,640	3.82	10	-32	40
1	R	Precuneus Cortex	3,640	4.91	6	-46	54
2	R	Angular Gyrus	880	5.03	60	-46	22
3	L	Lateral Occipital Cortex, superior division	544	4.06	-26	-80	34
4	L	Lateral Occipital Cortex, superior division	16	3.48	-18	-88	36

Table S5. Descriptive statistics for clusters and local extrema showing greater activation during the uncertain anticipation of benign versus threatening faces and voices (masked by the omnibus *F*-test), $p<.05$, whole-brain corrected.

Cluster	**Hemisphere**	**Label**	**mm³**	***t***	***x***	***y***	***z***
1	L	Intracalcarine Cortex	57,272	12.50	-12	-74	10
1	L	Occipital Pole	57,272	7.38	-2	-94	-4
1	R	Cuneal Cortex	57,272	5.92	2	-84	36
1	R	Intracalcarine Cortex	57,272	16.37	14	-78	12
1	R	Occipital Pole	57,272	6.87	14	-102	-2
2	R	Occipital Fusiform Gyrus	992	5.28	30	-68	-12
2	R	Temporal Occipital Fusiform Cortex	992	4.14	34	-60	-12
3	L	Lingual Gyrus	368	5.55	-16	-52	-12
4	R	Lateral Occipital Cortex, inferior division	8	3.37	40	-86	-10

Table S6. Descriptive statistics for clusters and local extrema showing greater activation during the certain anticipation of threatening faces and voices versus the uncertain anticipation of benign faces and voices (masked by the omnibus *F*-test), $p<.05$, whole-brain corrected.

Cluster	**Hemisphere**	**Label**	**mm³**	***t***	***x***	***y***	***z***
1	L	Lingual Gyrus	29,288	7.55	-6	-90	-10
1	L	Occipital Fusiform Gyrus	29,288	6.90	-28	-70	-12
1	L	Occipital Pole	29,288	5.25	-8	-98	2
1	L	Temporal Occipital Fusiform Cortex	29,288	6.26	-32	-56	-14
1	R	Cuneal Cortex	29,288	3.31	6	-86	38
1	R	Lingual Gyrus	29,288	7.98	6	-90	-6
1	R	Occipital Fusiform Gyrus	29,288	8.24	24	-76	-10
1	R	Occipital Pole	29,288	6.75	14	-98	2
1	R	Temporal Occipital Fusiform Cortex	29,288	5.49	28	-48	-12
2	L	Lateral Occipital Cortex, superior division	1,192	3.61	-12	-84	46
2	L	Occipital Pole	1,192	4.94	-14	-90	34
3	L	Precuneus Cortex	56	4.08	-4	-82	42

Table S7. Descriptive statistics for clusters and local extrema showing greater activation during the uncertain anticipation of benign faces and voices versus the certain anticipation of threatening faces and voices (masked by the omnibus *F*-test), $p<.05$, whole-brain corrected.

Cluster	**Hemisphere**	**Label**	**mm³**	***t***	***x***	***y***	***z***
1	R	Inferior Temporal Gyrus, temporooccipital part	21,888	4.84	56	-52	-12
1	R	Lateral Occipital Cortex, inferior division	21,888	9.05	46	-74	0
1	R	Middle Temporal Gyrus, temporooccipital part	21,888	5.74	54	-56	0
1	R	Temporal Occipital Fusiform Cortex	21,888	6.02	46	-56	-18
2	R	Lateral Occipital Cortex, superior division	5,040	4.00	38	-66	34
2	R	Postcentral Gyrus	5,040	4.11	14	-44	62
2	R	Superior Parietal Lobule	5,040	5.14	32	-40	64
2	R	Supramarginal Gyrus, posterior division	5,040	4.27	42	-40	50
3	R	Inferior Frontal Gyrus, pars opercularis	4,136	3.35	54	12	16
4	R	Intracalcarine Cortex	2,640	5.20	14	-76	12
5	L	Intracalcarine Cortex	2,408	4.37	-14	-76	12
6	R	Precentral Gyrus	2,352	5.54	12	-16	74
7	L	Lateral Occipital Cortex, inferior division	2,000	3.94	-48	-66	-18
7	L	Middle Temporal Gyrus, posterior division	2,000	3.64	-56	-42	-2
7	L	Middle Temporal Gyrus, temporooccipital part	2,000	4.30	-54	-50	4
7	L	Temporal Occipital Fusiform Cortex	2,000	4.20	-42	-60	-12
8	L	Precentral Gyrus	768	5.30	-32	-12	56
9	L	Superior Frontal Gyrus	624	5.07	-10	6	66

Table S8. Descriptive statistics for clusters and local extrema showing greater activation during the acute presentation of threatening faces and voices versus baseline, $p<.05$, whole-brain corrected.

Cluster	Hemisphere	Label	mm^3	*t*	*x*	*y*	*z*
1	R	Inferior Frontal Gyrus, pars triangularis	359,264	8.23	50	28	0
1	L	Frontal Operculum Cortex	359,264	10.89	-38	26	2
1	L	Frontal Orbital Cortex	359,264	11.11	-36	26	-4
1	L	Inferior Frontal Gyrus, pars opercularis	359,264	7.63	-48	20	16
1	R	Frontal Orbital Cortex	359,264	7.72	32	18	-18
1	L	Insular Cortex	359,264	7.73	-30	16	-14
1	R	Inferior Frontal Gyrus, pars opercularis	359,264	9.95	42	14	28
1	L	Putamen	359,264	5.82	-20	10	-6
1	R	Putamen	359,264	5.15	18	10	-2
1	L	Temporal Pole	359,264	15.29	-54	8	-12
1	L	Caudate	359,264	3.81	-8	8	6
1	R	Temporal Pole	359,264	16.33	52	8	-14
1	R	Precentral Gyrus	359,264	6	50	4	52
1	R	Superior Temporal Gyrus, anterior division	359,264	15.68	56	4	-14
1	R	Cingulate Gyrus, anterior division	359,264	5.3	6	2	28
1	L	Superior Temporal Gyrus, anterior division	359,264	17.11	-58	-4	-6
1	R	Amygdala	359,264	7.94	30	-4	-20
1	L	Amygdala	359,264	8.17	-30	-6	-22
1	L	Amygdala	359,264	8.22	-16	-6	-14
1	R	Amygdala	359,264	8.51	16	-6	-14
1	R	Amygdala	359,264	7.43	28	-8	-14
1	R	Planum Temporale	359,264	17.87	62	-10	2
1	L	Amygdala	359,264	6.85	-26	-12	-12
1	R	Heschls Gyrus (includes H1 and H2)	359,264	15.44	50	-14	4
1	R	Superior Temporal Gyrus, posterior division	359,264	14.11	68	-18	6
1	L	Heschls Gyrus (includes H1 and H2)	359,264	18.13	-48	-20	6
1	L	Planum Temporale	359,264	17.04	-60	-22	4
1	L	Inferior Temporal Gyrus, posterior division	359,264	6.33	-44	-26	-20
1	R	Brain Stem	359,264	11.88	12	-26	-10
1	L	Thalamus	359,264	12.47	-18	-30	-4
1	L	Brain Stem	359,264	9.42	-8	-30	-6

1	R	Thalamus	359,264	10.09	10	-30	-2
1	R	Temporal Fusiform Cortex, posterior division	359,264	12	38	-38	-24
1	L	Supramarginal Gyrus, posterior division	359,264	15.34	-66	-42	12
1	L	Lingual Gyrus	359,264	6.05	-16	-46	-8
1	R	Lingual Gyrus	359,264	9.11	18	-46	-10
1	L	Temporal Occipital Fusiform Cortex	359,264	13.73	-38	-48	-20
1	R	Temporal Occipital Fusiform Cortex	359,264	16.56	36	-56	-16
1	L	Intracalcarine Cortex	359,264	11.22	-20	-68	6
1	R	Precuneus Cortex	359,264	5.76	12	-74	40
1	R	Occipital Fusiform Gyrus	359,264	15.57	30	-76	-10
1	R	Cuneal Cortex	359,264	6.57	4	-80	36
1	L	Occipital Fusiform Gyrus	359,264	16.68	-26	-84	-12
1	L	Occipital Pole	359,264	17.4	-14	-96	-12
1	R	Occipital Pole	359,264	18.68	14	-98	0
2	L	Paracingulate Gyrus	12,936	7.09	-10	20	38
2	L	Superior Frontal Gyrus	12,936	5.25	-10	20	68
2	R	Paracingulate Gyrus	12,936	4.26	10	20	40
2	R	Superior Frontal Gyrus	12,936	5.14	8	18	68
3	R	Frontal Pole	2,784	3.99	10	60	36
3	L	Superior Frontal Gyrus	2,784	6.1	-2	56	32
3	R	Superior Frontal Gyrus	2,784	4.83	6	50	40
4	L	Frontal Pole	2,008	3.77	-4	58	-18
4	B	Frontal Medial Cortex	2,008	5.12	0	42	-24
4	L	Frontal Medial Cortex	2,008	5.31	-2	32	-28

Table S9. Descriptive statistics for clusters and local extrema showing greater activation during the acute presentation of benign faces and voices versus baseline, $p<.05$, whole-brain corrected.

Cluster	Hemisphere	Label	mm^3	*t*	*x*	*y*	*z*
1	L	Frontal Orbital Cortex	313,816	9.69	-34	28	0
1	L	Insular Cortex	313,816	9.61	-30	26	0
1	R	Inferior Frontal Gyrus, pars triangularis	313,816	9.00	52	26	20
1	L	Inferior Frontal Gyrus, pars triangularis	313,816	6.29	-52	24	4
1	R	Frontal Orbital Cortex	313,816	7.08	42	24	-8
1	L	Inferior Frontal Gyrus, pars opercularis	313,816	7.95	-50	18	24
1	R	Inferior Frontal Gyrus, pars opercularis	313,816	10.43	48	18	28
1	R	Middle Frontal Gyrus	313,816	10.37	46	16	30
1	R	Temporal Pole	313,816	14.54	48	14	-18
1	L	Temporal Pole	313,816	18.12	-54	6	-10
1	R	Precentral Gyrus	313,816	4.83	46	4	46
1	R	Superior Temporal Gyrus, anterior division	313,816	18.13	56	4	-14
1	R	Amygdala	313,816	7.46	26	2	-18
1	L	Amygdala	313,816	6.95	-28	0	-20
1	R	Amygdala	313,816	7.43	30	-2	-24
1	R	Amygdala	313,816	8.00	32	-4	-20
1	L	Superior Temporal Gyrus, anterior division	313,816	17.79	-56	-6	-4
1	L	Amygdala	313,816	9.18	-16	-6	-14
1	L	Amygdala	313,816	7.58	-30	-6	-22
1	R	Amygdala	313,816	5.37	28	-12	-12
1	R	Superior Temporal Gyrus, posterior division	313,816	15.69	50	-16	-6
1	R	Heschls Gyrus (includes H1 and H2)	313,816	13.72	52	-18	6
1	L	Heschls Gyrus (includes H1 and H2)	313,816	15.94	-46	-20	6
1	L	Planum Temporale	313,816	16.62	-60	-22	6
1	R	Brain-Stem	313,816	10.19	10	-26	-8
1	L	Thalamus	313,816	12.39	-20	-30	-4
1	R	Thalamus	313,816	9.41	10	-30	-2
1	L	Parietal Operculum Cortex	313,816	4.79	-34	-34	22
1	L	Cingulate Gyrus, posterior division	313,816	5.25	-6	-38	26
1	R	Temporal Fusiform Cortex, posterior division	313,816	11.52	38	-38	-24
1	R	Supramarginal Gyrus, posterior division	313,816	13.61	54	-40	10

1	L	Supramarginal Gyrus, posterior division	313,816	12.37	-66	-42	12
1	L	Temporal Fusiform Cortex, posterior division	313,816	12.04	-40	-42	-22
1	R	Lingual Gyrus	313,816	6.34	18	-48	-8
1	L	Temporal Occipital Fusiform Cortex	313,816	12.77	-36	-50	-18
1	L	Lingual Gyrus	313,816	4.72	-16	-50	-8
1	R	Temporal Occipital Fusiform Cortex	313,816	14.47	36	-54	-16
1	R	Precuneus Cortex	313,816	4.97	14	-66	40
1	R	Intracalcarine Cortex	313,816	6.19	12	-68	14
1	L	Intracalcarine Cortex	313,816	9.99	-20	-70	8
1	R	Occipital Fusiform Gyrus	313,816	16.57	32	-78	-12
1	R	Cuneal Cortex	313,816	4.36	2	-80	36
1	L	Occipital Fusiform Gyrus	313,816	15.49	-26	-84	-12
1	L	Occipital Pole	313,816	16.92	-10	-94	-10
1	R	Occipital Pole	313,816	17.94	14	-98	0
2	R	Superior Frontal Gyrus	10,680	5.69	6	24	58
2	R	Paracingulate Gyrus	10,680	3.57	10	24	32
2	L	Paracingulate Gyrus	10,680	5.18	-10	20	38
2	L	Superior Frontal Gyrus	10,680	4.01	-10	18	68
3	R	Thalamus	968	6.33	6	-8	6

Table S10. Descriptive statistics for clusters and local extrema showing greater activation during the acute presentation of threatening versus benign faces and voices, $p<.05$, whole-brain corrected.

Cluster	Hemisphere	Label	mm^3	*t*	*x*	*y*	*z*
1	L	Intracalcarine Cortex	54,808	7.60	-16	-70	6
1	L	Lateral Occipital Cortex, inferior division	54,808	5.06	-40	-72	-8
1	L	Occipital Fusiform Gyrus	54,808	5.21	-34	-68	-18
1	L	Occipital Pole	54,808	5.96	-4	-100	-2
1	L	Temporal Occipital Fusiform Cortex	54,808	4.88	-32	-56	-16
1	R	Cuneal Cortex	54,808	4.56	18	-74	30
1	R	Intracalcarine Cortex	54,808	6.73	14	-66	10
1	R	Lateral Occipital Cortex, inferior division	54,808	4.75	36	-86	-10
1	R	Lingual Gyrus	54,808	6.55	4	-88	-2
1	R	Occipital Fusiform Gyrus	54,808	6.23	36	-68	-14
1	R	Occipital Pole	54,808	7.00	4	-90	4
1	R	Precuneus Cortex	54,808	5.64	18	-72	38
1	R	Temporal Fusiform Cortex, posterior division	54,808	4.05	36	-36	-24
1	R	Temporal Occipital Fusiform Cortex	54,808	5.82	36	-54	-14
2	R	Planum Temporale	10,504	5.35	38	-32	14
2	R	Superior Temporal Gyrus, posterior division	10,504	6.50	50	-16	-6
2	R	Supramarginal Gyrus, posterior division	10,504	4.75	68	-38	16
3	L	Central Opercular Cortex	7,128	3.51	-62	-14	10
3	L	Heschls Gyrus (includes H1 and H2)	7,128	4.75	-44	-24	8
3	L	Planum Temporale	7,128	5.77	-38	-34	10
3	L	Supramarginal Gyrus, posterior division	7,128	4.28	-66	-42	18
4	L	Frontal Orbital Cortex	3,264	5.07	-28	14	-18
4	L	Left Putamen	3,264	4.81	-22	8	-8
5	L	Cingulate Gyrus, posterior division	2,832	5.51	-2	-16	40
5	R	Cingulate Gyrus, posterior division	2,832	5.49	6	-24	28
6	R	Temporal Pole	2,816	5.44	54	8	-16
7	L	Brain-Stem	2,256	5.05	-6	-36	-6
7	R	Brain-Stem	2,256	4.51	12	-26	-10
8	L	Left Caudate	1,992	3.60	-8	8	14
9	L	Frontal Pole	1,416	4.24	-6	58	18
10	R	Frontal Orbital Cortex	1,400	4.93	32	18	-20
10	R	Right Putamen	1,400	4.47	26	12	-6
11	R	Precentral Gyrus	1,200	5.15	52	-2	48
12	L	Inferior Frontal Gyrus, pars opercularis	800	3.98	-48	20	10

Table S11. Descriptive statistics for clusters and local extrema showing greater activation during the acute presentation of benign versus threatening faces and voices, $p<.05$, whole-brain corrected.

Cluster	**Hemisphere**	**Label**	**mm³**	***t***	***x***	***y***	***z***
1	L	Angular Gyrus	8,464	3.85	-44	-60	24
1	L	Lateral Occipital Cortex, superior division	8,464	6.42	-42	-78	30
2	L	Middle Frontal Gyrus	6,680	3.94	-38	10	62
2	L	Superior Frontal Gyrus	6,680	5.44	-24	14	60
3	L	Precuneus Cortex	5,968	6.86	-6	-54	16
3	R	Precuneus Cortex	5,968	4.82	8	-54	6
4	L	Cingulate Gyrus, posterior division	4,576	5.38	-6	-38	36
4	L	Precuneus Cortex	4,576	4.74	-2	-54	48
4	R	Lateral Occipital Cortex, superior division	4,576	3.84	12	-60	60
4	R	Precuneus Cortex	4,576	5.40	10	-60	50
4	R	Superior Parietal Lobule	4,576	3.80	12	-54	66
5	R	Lateral Occipital Cortex, superior division	2,920	6.61	46	-70	34
6	L	Lateral Occipital Cortex, superior division	2,896	4.55	-8	-64	62
6	L	Postcentral Gyrus	2,896	3.99	-8	-48	70
6	L	Precuneus Cortex	2,896	4.23	-8	-66	56
7	L	Middle Temporal Gyrus, temporooccipital part	2,208	5.62	-58	-50	-6
8	L	Parahippocampal Gyrus, posterior division	2,128	5.20	-28	-30	-18
8	L	Temporal Fusiform Cortex, posterior division	2,128	5.83	-26	-38	-18
9	R	Frontal Pole	1,232	4.12	28	36	50
9	R	Superior Frontal Gyrus	1,232	4.11	22	30	42
10	R	Middle Frontal Gyrus	1,000	3.96	26	16	54

Table S12. Descriptive statistics for clusters and local extrema showing greater activation during the temporally uncertain versus certain presentation of benign faces and voices, $p<.05$, whole-brain corrected.

Cluster	**Hemisphere**	**Label**	**mm³**	***t***	***x***	***y***	***z***
1	L	Inferior Temporal Gyrus, temporooccipital part	6,664	5.96	-42	-54	-8
1	L	Lateral Occipital Cortex, inferior division	6,664	4.84	-40	-70	-6
1	L	Temporal Occipital Fusiform Cortex	6,664	5.78	-34	-48	-16
2	L	Superior Frontal Gyrus	4,200	4.29	-4	36	46
2	R	Cingulate Gyrus, anterior division	4,200	3.60	6	16	34
2	B	Juxtapositional Lobule Cortex	4,200	3.93	0	6	48
2	R	Paracingulate Gyrus	4,200	4.90	8	18	44
3	L	Occipital Pole	4,176	3.69	-2	-90	26
3	L	Precuneus Cortex	4,176	4.23	-10	-68	42
3	R	Lateral Occipital Cortex, superior division	4,176	3.52	10	-84	44
3	R	Occipital Pole	4,176	4.80	18	-98	24
3	R	Precuneus Cortex	4,176	3.62	4	-76	48
4	R	Superior Parietal Lobule	3,424	4.58	30	-42	42
4	R	Supramarginal Gyrus, posterior division	3,424	4.98	48	-38	48
5	R	Lateral Occipital Cortex, inferior division	2,696	3.37	40	-78	-12
5	R	Temporal Occipital Fusiform Cortex	2,696	5.23	36	-48	-18
6	R	Precuneus Cortex	2,504	5.06	10	-72	36
7	L	Precentral Gyrus	2,328	4.54	-48	0	36
8	R	Frontal Operculum Cortex	1,424	4.61	48	12	0
8	R	Insular Cortex	1,424	4.20	34	20	6
9	L	Frontal Operculum Cortex	1,344	3.83	-40	14	2
9	L	Insular Cortex	1,344	4.81	-30	18	10
10	R	Precentral Gyrus	1,176	4.55	48	6	32

Table S13. Descriptive statistics for clusters and local extrema showing greater activation during the temporally certain versus uncertain presentation of benign faces and voices, $p<.05$, whole-brain corrected.

Cluster	**Hemisphere**	**Label**	**mm³**	***t***	***x***	***y***	***z***
1	R	Planum Temporale	2,640	4.60	58	-16	4
1	R	Superior Temporal Gyrus, anterior division	2,640	4.17	62	0	-6
1	R	Superior Temporal Gyrus, posterior division	2,640	4.61	68	-22	4
2	L	Heschls Gyrus (includes H1 and H2)	2,008	4.81	-52	-18	4
2	L	Planum Temporale	2,008	3.90	-62	-18	4
2	L	Superior Temporal Gyrus, anterior division	2,008	4.43	-62	-6	-6
2	L	Superior Temporal Gyrus, posterior division	2,008	4.40	-64	-12	2
3	L	Frontal Medial Cortex	1,104	4.75	-8	42	-12
3	L	Frontal Pole	1,104	4.38	-6	58	-16
3	B	Frontal Medial Cortex	1,104	4.05	0	42	-16

Table S14. Descriptive statistics for clusters and local extrema showing a significant positive Valence × Temporal Certainty interaction during the acute presentation of faces and voices (Uncertain Threat—Uncertain Safety > Certain Threat—Certain Safety), $p<.05$, whole-brain corrected.

Cluster	**Hemisphere**	**Label**	**mm³**	***t***	***x***	***y***	***z***
1	L	Lateral Occipital Cortex, superior division	5,160	5.18	-14	-66	60
1	L	Precuneus Cortex	5,160	5.26	-8	-64	52
1	R	Precuneus Cortex	5,160	5.36	10	-58	56
2	L	Pregenual anterior cingulate cortex	4,408	4.53	-2	38	12
2	R	Pregenual anterior cingulate cortex	4,408	4.81	4	36	14
2	R	Frontal Medial Cortex	4,408	4.57	10	50	-8
2	R	Frontal Pole/Dorsolateral Prefrontal Cortex	4,408	4.38	8	58	8
2	R	Paracingulate Gyrus	4,408	3.54	6	34	-10
3	L	Postcentral Gyrus	4,272	4.40	-50	-20	36
3	L	Supramarginal Gyrus, anterior division	4,272	5.21	-62	-30	32
4	L	Precuneus Cortex	1,912	4.75	-16	-68	24
5	R	Angular Gyrus	1,416	5.02	50	-54	14
6	L	Central Opercular Cortex	1,336	3.58	-44	6	0
6	L	Insular Cortex	1,336	4.80	-38	-8	-10
7	L	Frontal Medial Cortex	984	4.73	-10	48	-10
7	L	Frontal Pole/Dorsolateral Prefrontal Cortex	984	3.96	-4	58	0
8	L	Inferior Frontal Gyrus, pars opercularis	896	4.92	-58	10	18
8	L	Precentral Gyrus	896	4.22	-58	6	28
9	R	Brain-Stem	872	4.24	12	-16	-22
9	R	Parahippocampal Gyrus, anterior division	872	4.26	18	-16	-24
9	R	Right Hippocampus	872	4.43	26	-22	-18
9	R	Temporal Fusiform Cortex, posterior division	872	3.45	34	-22	-24

Table S15. Descriptive statistics for clusters and local extrema showing a significant negative Valence × Temporal Certainty interaction during the acute presentation of faces and voices (Uncertain Threat—Uncertain Safety < Certain Threat—Certain Safety), $p<.05$, whole-brain corrected.

Cluster	**Hemisphere**	**Label**	**mm³**	***t***	***x***	***y***	***z***
1	L	Intracalcarine Cortex	65,456	12.80	-16	-72	6
1	L	Lingual Gyrus	65,456	8.43	-18	-68	-4
1	L	Occipital Pole	65,456	7.24	-6	-98	-4
1	L	Cuneal Cortex	65,456	6.62	-2	-88	34
2	R	Intracalcarine Cortex	65,456	12.58	18	-68	8
1	B	Lingual Gyrus	65,456	11.50	0	-88	-4
1	R	Supracalcarine Cortex	65,456	11.24	2	-74	12
1	R	Cuneal Cortex	65,456	7.38	8	-84	36
1	R	Occipital Pole	65,456	7.09	12	-104	2

Table S16. Descriptive statistics for clusters and local extrema showing greater activation during the uncertain versus certain presentation of threatening faces and voices (masked by the Valence × Certainty contrast), $p<.05$, whole-brain corrected.

Cluster	**Hemisphere**	**Label**	**mm³**	***t***	***x***	***y***	***z***
1	L	Postcentral Gyrus	1,640	4.04	-50	-20	34
1	L	Supramarginal Gyrus, anterior division	1,640	4.69	-62	-28	34
2	R	Pregenual anterior cingulate cortex	840	4.95	6	38	14
3	L	Precentral Gyrus	816	5.15	-58	8	16
4	L	Lateral Occipital Cortex, superior division	696	3.62	-14	-68	56
5	L	Precuneus Cortex	672	4.74	-16	-66	24
6	L	Central Opercular Cortex	312	3.57	-48	8	0
6	L	Insular Cortex	312	4.76	-38	-8	-12

Table S17. Descriptive statistics for clusters and local extrema showing greater activation during the uncertain presentation of threatening versus benign faces and voices (masked by the Valence × Certainty contrast), $p<.05$, whole-brain corrected.

Cluster	**Hemisphere**	**Label**	**mm³**	***t***	***x***	***y***	***z***
1	L	Pregenual anterior cingulate cortex	1,752	5.04	-2	36	-4
1	R	Pregenual anterior cingulate cortex	1,752	4.66	6	40	10
2	L	Central Opercular Cortex	288	4.61	-62	-20	12
3	R	Frontal Pole/Dorsolateral Prefrontal Cortex	128	3.71	6	56	8
4	L	Supramarginal Gyrus, anterior division	120	3.31	-64	-38	24
5	L	Paracingulate Gyrus	40	3.64	-8	46	-2

Table S18. Descriptive statistics for clusters and local extrema showing greater activation during the uncertain presentation of threatening versus the certain presentation of benign faces and voices (masked by the Valence × Certainty contrast), $p<.05$, whole-brain corrected.

Cluster	**Hemisphere**	**Label**	**mm³**	***t***	***x***	***y***	***z***
1	R	Brain-Stem	8	3.60	10	-18	-20
2	L	Precentral Gyrus	8	3.28	-58	6	32

Table S19. Descriptive statistics for clusters and local extrema showing greater activation during the uncertain presentation of benign versus the certain presentation of threatening faces and voices (masked by the Valence × Certainty contrast), $p<.05$, whole-brain corrected.

Cluster	**Hemisphere**	**Label**	**mm³**	***t***	***x***	***y***	***z***
1	L	Precuneus Cortex	968	4.97	-12	-64	26
2	R	Precuneus Cortex	712	4.33	8	-58	52
3	L	Precuneus Cortex	8	3.32	-2	-62	18

Table S20. Descriptive statistics for clusters and local extrema showing greater activation during the certain presentation of benign versus the uncertain presentation of threatening faces and voices (masked by the Valence × Certainty contrast), $p<.05$, whole-brain corrected.

Cluster	**Hemisphere**	**Label**	**mm³**	***t***	***x***	***y***	***z***
1	L	Precuneus Cortex	648	5.57	-6	-56	16
2	L	Lateral Occipital Cortex, superior division	408	4.06	-16	-66	64
3	L	Frontal Medial Cortex	64	4.51	-6	46	-12
4	L	Precuneus Cortex	8	3.30	-8	-66	22

Table S21. Descriptive statistics for clusters and local extrema showing greater activation during the certain presentation of benign versus threatening faces and voices (masked by the Valence × Certainty contrast), $p<.05$, whole-brain corrected.

Cluster	**Hemisphere**	**Label**	**mm³**	***t***	***x***	***y***	***z***
1	L	Lateral Occipital Cortex, superior division	5,104	6.24	-12	-64	60
1	L	Precuneus Cortex	5,104	6.21	-2	-56	48
1	R	Precuneus Cortex	5,104	6.47	10	-60	52
2	L	Postcentral Gyrus	2,440	4.31	-58	-24	40
2	L	Supramarginal Gyrus, anterior division	2,440	5.34	-62	-28	32
3	L	Precuneus Cortex	1,840	7.28	-6	-54	18
4	R	Parahippocampal Gyrus, anterior division	744	5.45	18	-16	-24
4	R	Right Hippocampus	744	6.18	26	-20	-18
5	L	Frontal Medial Cortex	472	4.19	-8	48	-10
5	L	Frontal Pole/Dorsolateral Prefrontal Cortex	472	3.61	-4	56	-2
5	B	Frontal Medial Cortex	472	3.69	0	52	-8
6	R	Frontal Medial Cortex	336	4.66	10	54	-8
7	R	Angular Gyrus	184	3.94	44	-56	22
8	R	Paracingulate Gyrus	8	3.25	8	42	-10

Table S22. Descriptive statistics for clusters and local extrema showing greater activation during the certain versus uncertain presentation of benign faces and voices (masked by the Valence × Certainty contrast), $p<.05$, whole-brain corrected.

Cluster	**Hemisphere**	**Label**	**mm³**	***t***	***x***	***y***	***z***
1	L	Lateral Occipital Cortex, superior division	1,248	4.76	-14	-66	62
1	L	Precuneus Cortex	1,248	3.77	-8	-58	62
2	R	Pregenual anterior cingulate cortex	1,040	4.02	6	40	-2
2	R	Frontal Medial Cortex	1,040	5.05	10	50	-8
3	L	Frontal Medial Cortex	984	5.88	-6	48	-12
4	R	Angular Gyrus	816	4.52	52	-56	16
5	L	Precuneus Cortex	688	4.35	-8	-56	10
6	R	Precuneus Cortex	632	4.38	12	-58	58
7	L	Central Opercular Cortex	232	3.97	-62	-18	14
8	R	Frontal Pole/Dorsolateral Prefrontal Cortex	152	4.14	10	62	0
9	L	Pregenual anterior cingulate cortex	104	4.13	-4	36	-6